MAGNETIC TEMPERATURE ESTIMATION USING A MODIFIED SINGLE-PHASE TRANSFORMER CORE

By

Daniel Fernández Alonso

Submitted to the Department of Electrical Engineering, Electronics,

Computers and Systems

In partial fulfilment of the requirements for the degree of

Master of Science in Electrical Energy Conversion and Power Systems

At The

UNIVERSIDAD DE OVIEDO

July 2013

Author ……

Daniel Fenández Alonso

Certified by ……

David Díaz Resigosa

MAGNETIC TEMPERATURE ESTIMATION USING A MODIFIED SINGLE-PHASE TRANSFORMER CORE

By

Daniel Fernández Alonso

Submitted to the Department of Electrical Engineering, Electronics, Computers and Systems
on July 22, 2013, in partial fulfilment of the
requirements for the degree of
Master of Science in Electrical Energy Conversion and Power Systems

Index

Introduction

Permanent magnet synchronous machines are widely used in industry and they are ofthen best solution for some applications such as traction, electric vehicle, robotics or aerospace applications. One of the most common types of rare earth magnet used to build permanent magnets synchronous machine is neodymium-iron-bore (NdFeB). When a magnet is subject to magnetic field variations, eddy currents are induced and its temperature will increase accordingly [1]. The performance of PM machines is strongly influenced by the magnets' temperature due to the temperature dependency of its properties. An increase of the magnet temperature can result in a reduction of the magnet strength (see Fig1.1), either transiently or permanently, which translates into a reduced torque production capability of the machine. Therefore, having accurate measurement or estimates of the magnet temperature is highly desirable in many applications.

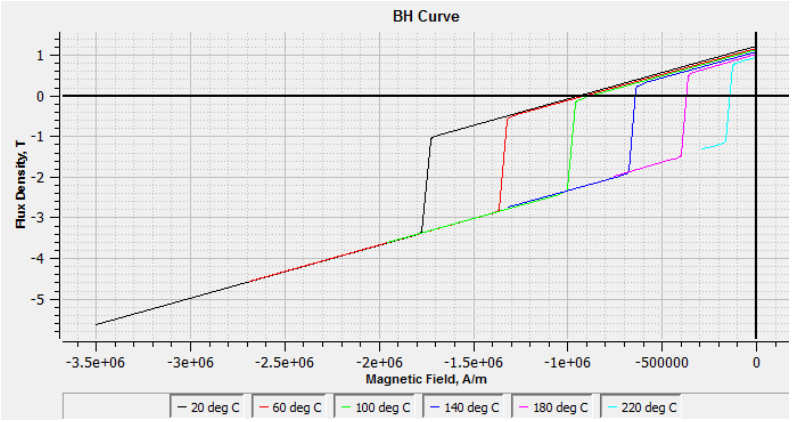

Fig 1.1 N36SH magnet curves for different temperatures. SOURCE: J-MAG Designer

This process is reversible as long as the demagnetizing force, to which the magnet is exposed, does not reach the magnet specific knee value. Reversibility means that the flux density will grow to its original value when the temperature is reduced again. But the reduction in the rotor flux linkage due to temperature will lead directly to lower electromagnetic torque [4]. In a torque control, rotor flux variations can be compensated having a flux observer or having the magnet temperature.

As the important variable to measure is the magnets temperature and rotor is continuously turning, this task becomes very complicated. Some techniques have been used to extract data such as infrared sensors [3], wireless sensors [4] or slip rings [5]. Several methods have been developed in recent years to estimate magnets temperature to compensate demagnetization. By injecting high frequency signals in the motor, magnets resistance variations can be obtained and therefore temperature variations [6].

The aim of this project is to design and develop a simplified system, where e estimation methods can be easily tested and verify results with sensors, having no moving parts. A modified transformer will work as simplified motor and it will be demonstrated that the results are similar than in permanent magnet motor.

1. Objectives of the Master Thesis

The purpose of this Master thesis is to develop an experimental setup and a methodology to evaluate the impact on the temperature of the current/voltage waveforms applied to the machine by the power converter, and eventually in the magnet properties.

For the experimental setup, a single-phase commercial transformer will be used. An airgap will be performed in the transformer core. The permanent magnet being tested will be placed within this airgap (resembling the configuration of the magnet within a PMSM). Multiple temperature sensors types will be placed to precisely monitor the magnet temperature, the corresponding measuring, conditioning and transmission circuits will be developed. The primary/secondary transformer winding will be fed by an H-bridge power converter, also to be developed for this project. Impact of the waveforms applied by the power converter on the magnet temperature will be studied, with the final goal of extending the conclusions to the PMSM magnet temperature behaviour.

2. State of the art

Many studies have been carried out concern to eddy current losses in magnets [7]-[8]. And it was demonstrated that rotor losses in permanent magnet synchronous motors are mainly due to eddy and hysteresis losses. High torque and speed operation increases rotor losses, It could be acceptable for many applications to have just losses, but the problem does not finish there, the energy lost is rotor goes as heat. And due to magnet properties, heat makes magnet to loose strength and may drive to reach thermal demagnetization.

Mainly three ways have been under study trying to know magnets temperature: thermal models of the machine [10], temperature estimation methods [6] and direct measurement systems [4].

The proposed thermal equivalent models of PM machines have high dependent of geometry and cooling systems and usually require calibration for each machine design and the consequence is a limited accuracy. Some other research studies integrate temperature sensors directly within the motor attached to the parts to be measured. This system may work properly helping the control system to correct currents as function of the motor temperature to keep the desired torque. Integrating sensors in the rotor as well as building a wireless system to get the data, has de inconvenience of the price, making the assembly process complicated as well.

To overcome price disadvantages of the sensing system, and the inaccuracy of the thermal model, another method to estimate magnet temperature by injecting high frequency signals was discovered recent years [6]. In this method a high frequency signal superimposed to the fundamental excitation is injected to calculate stator high frequency impedance. A variation of the magnet temperature will produce a variation of its resistance following the Callendar–Van Dusen equation.

In this project a simplified method is used to quantify how eddy currents affects to the rotor temperature, which frequencies makes the magnets to get hot faster and where is the boundary where frequency does not heat the magnet but skin effect appears. The relationship between this model and a real motor will be explained as well.

Some studies have been done with a similar model [4] but the aim of the study has been slightly different. Closed type measurement equipment was built by which AC loss (eddy currents and hysteresis losses) were measured. The conclusion if this study was that hysteresis losses are twice eddy losses in some situations.

3. Modified single phase transformer

Using a single phase transformer, current through the coil is converted to magnetic flux through the core, varying at same frequency with proportional amplitudes. For this experiment magnet within a magnetic flux variation is needed, to analyse how its properties change. A single phase transformer as the shown in the Fig 4.1, was modified to insert a magnet on its air gap and also the core was modified to drive all flux lines through the magnet (Fig 4.2).

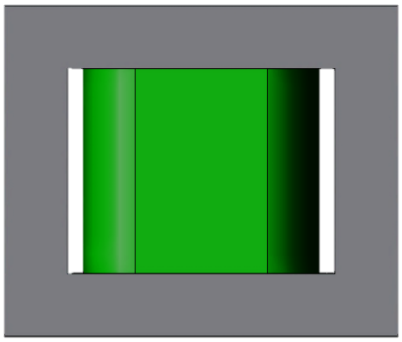

Fig 4.1. Commercial transformer appearance

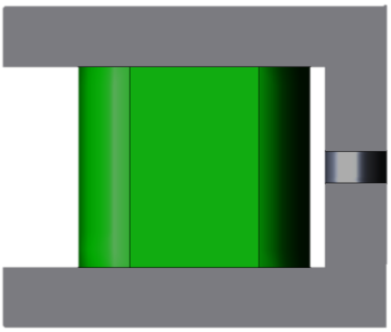

Fig4.2. Transformer appearance after modification

It is a commercial transformer, with 4 coils: two for primary and two for secondary with ratio (4.1). During the experiments the transformer is feed on the secondary side to reduce risks, as the same magnetic field can be created in both sides.

$$r = \frac{380}{8} = 47.5 \tag{4.1}$$

Nominal power of the transformer must be a known value to later design the proper inverter. There is not characteristic sheet about the transformer or other information so the way to characterize the transformer is by measuring its impedance at 50 Hz. It will always works above that frequency for these experiments. As it is well known, that impedance in a transformer increases with frequency (4.2) since it is almost pure inductive.

$$X_L = 2\pi f L \tag{4.2}$$

To carry out the experiments, it will not be necessary to design an inverter adjusted to the transformer nominal values since just weak high frequency signals will be injected in the transformer.

3.1.Principle of operation

The electrical model of a typical transformer is a well know circuit, where both copper and iron losses are represented, as in Fig4.1. Where Vp, Vs and Ip,Is are the voltage and currents at the primary and secondary side respectively. Winding joule losses and leakage reactances are represented by Rp and Xp at the primary side and Xs' and Rs' at the secondary side referred to primary. Finally core or iron losses and magnetizing reactance Xm are represented by Rc and Xm. The normal operation of a transformer like in the Fig4.1 can be studied with this model for both transient and steady state.

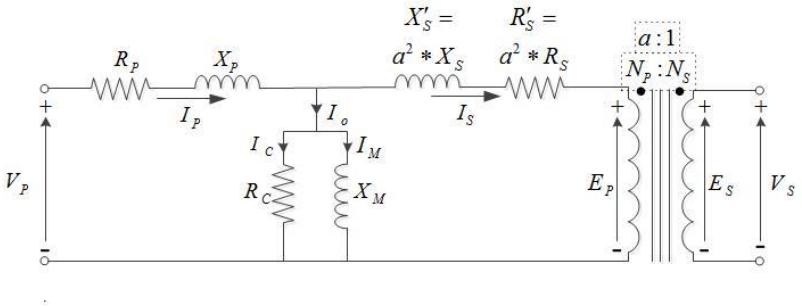

Fig4.3. Electrical model of a transformer

When the transformer is modified as in Fig4.2 the electric model will change as well. First change introduced to the transformer is that one column of the E core has been removed. With this change, all the magnetic flux is driven through the remaining column. Looking at the circuit above it can be appreciate that the topology does not change yet, juts core resistance and impedance increases. Leakage reactance Xm will change as well as core losses.

Next change introduced is the creation of an air-gap in the middle of the remaining current to later introduce a magnet. Transformer will be feed at the primary, secondary windings will remain opened and the magnet inserted in the air-gap will alter the circuit topology. To study the transformer now, the circuit to be studied is shown on Fig4.4.

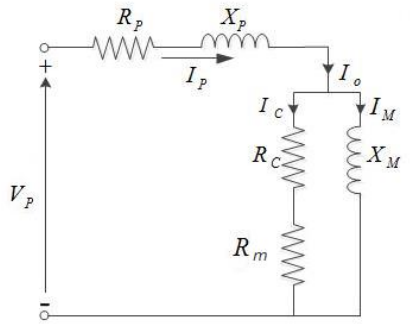

Fig4.4. Electrical model of a modified transformer

Magnet resistance is the important one in the circuit above. To know its value primary winding resistance must be known as well as core loss resistance. The total impedance of

the circuit can be known measuring current and voltage waveforms at the input. To be more precise, voltage and current signals are decomposed applying the fast Fourier transform which gives also phase of each signal. Taking the voltage and current signals at the proper frequency, total impedance of the transformer is indirectly calculated. Its real part represents the resistance that is given by (4.3)

$$R_{total} = R_{core} + R_{coil} + R_{magnet} \tag{4.3}$$

Magnet resistance can be considered much higher than core resistance as core is laminated eddy currents are reduced while magnet is susceptible to have higher eddy currents.

For both magnet and coil, resistance is going to vary according to the Callendar–Van Dusen equation (4.4) where R_0 is the resistance at T_0, R is the temperature at T and α is the temperature coefficient at 0°.

$$R = R_0 * \left(1 + \alpha * (T - T_0)\right) \tag{4.4}$$

To carry out the experiments, temperature variations in the coil will be registered and the resistance at ambient temperature will be calculated. The parameter α comes given by the copper temperature coefficient: 0.0043.

4. Single phase inverter

For this experiment, current control is not needed. However, it is necessary a system able to feed the transformer with a customizable sinusoidal waveform, in both amplitude and frequency. That can be achieved by using an H-bridge Fig5.1. The block diagrams of the system is explained in the following sections but the full schematic and PCB for the system, can be found on attached. In schematic and PCB section, document number one shows the schematic of the h-bridge (sheets 1 and 2) and H-Bridge PCB (sheets 3, 4 and 5).

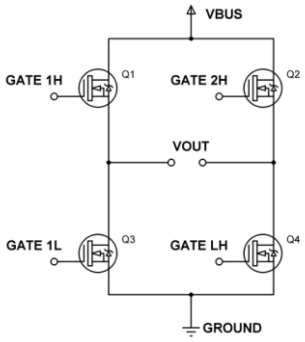

Fig5. 1. H-bridge power stage schematic

4.1. Devices selection for power side

Nominal values of the transformer would limit the minimum power of the inverter, but those values are unknown. What it is well known is that in the experiment, high frequency signals will be injected only. The most important parts at the power side are switching devices. For this application, both mosfet and IGBT technologies can fulfil the design requirements: switching frequency up to 20 KHz (typically 5 KHz), and peak voltage at primary side 538 Volts. The maximum current for injected signals will be around 8 amps peak. With these specifications, the selected MOSFET is the STB21N65M5 from ST Microelectronics. It is a low cost MOSFET and may handle up to 650 V, 17 Amperes. It has low R_{DS}(on).

To solve ground problems when gating MOSFET, commercial driver is installed in the power circuit. L6390 driver from ST Microelectronics, is a voltage gate driver IC suitable for inverter applications, able to command one branch of two switches and it can work up to 600

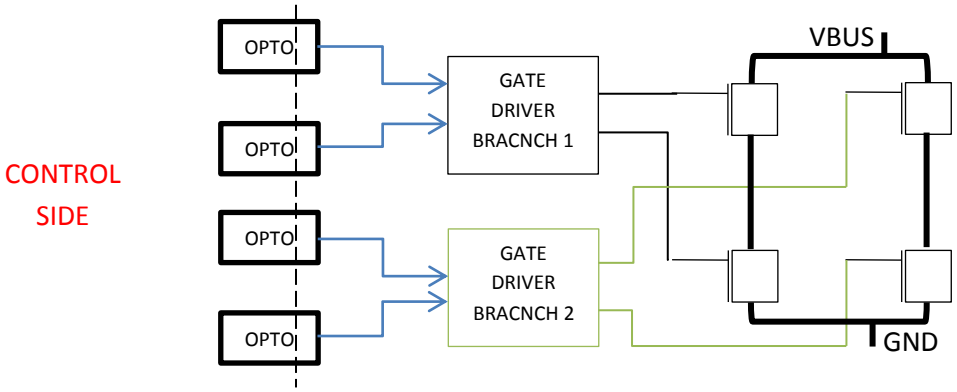

Fig5. 2. H-bridge power stage block diagram

volts. It can be commanded with 3.3 to 5 volts TTL signals and integrates the bootstrap diode. Bootstrap capacitor is the only external component required. It can be enabled by hardware and integer overcurrent disconnection. Fig5.2 summarizes power side of the PCB.

The L6390 gate driver offers the possibility to be commanded with just one control signal, because input for low side control is internally inverted. But it is necessary to add some components to set dead time. This function will not be used since the microcontroller has an internal dead time generator block, which may be configured by software, reducing costs and increasing flexibility.

4.2. Devices selection for control side

Control system for the h-bridge includes a microcontroller, the interface between control signals and power signals and also, a communication port to facilitate settings of amplitude and frequency to be generated.

Many microcontrollers can handle an H-bridge but the chosen for this project is a DSC from microchip: dsPIC30f6010a. It is 16 bit a low cost device, designed for motor control, signal filtering and able to work up to 120 MHz. It includes internal RC clock calibrated to easily generate communication frequencies multiples.

Power side is isolated by means of fast optocouplers. These devices connect signals coming from the DSC with mosfet gate drivers, as a protection. Besides, optocouplers adapt voltages: at the DSC side control signals vary from 0 to 5 volts, while 0 to 20 volts signals are necessary to command some kinds of mosfet gate driver. HCPL-2201 optocoupler is chosen to this task as it is recommended by the manufacturer for these kinds of applications, able to adapt voltages as well.

Communication block is referred to the same ground and a buffer is used to increase to boost the maximum current given by the DSC pins when needed. A standard DB-9 connector is chosen since it is a RS232 interface. Other connector is used to program and debug software in the microcontroller. Fig5.3 summarizes control side of the PCB.

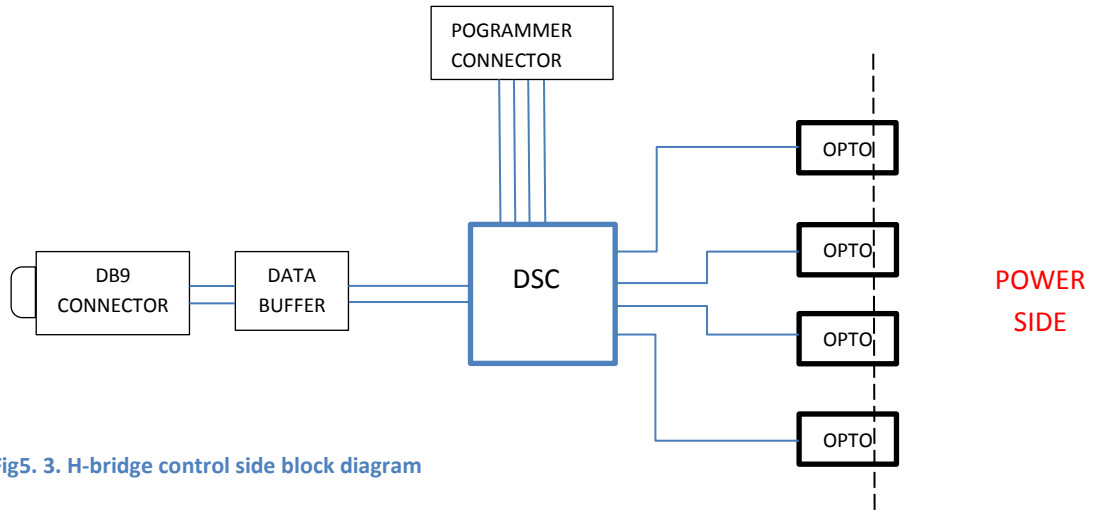

Fig5. 3. H-bridge control side block diagram

4.3. Control strategies for the H-bridge

The H-bridge enables a voltage to be applied across the load in either direction. With the simplest control, a square signal can be easily obtained, but having high harmonic content (odd-integer harmonic frequencies) as shown on Fig5.4.

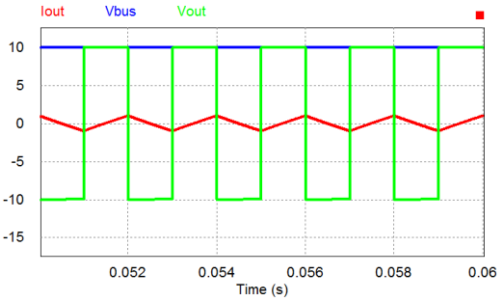

Fig5.4. Square waveform for H-bridge control

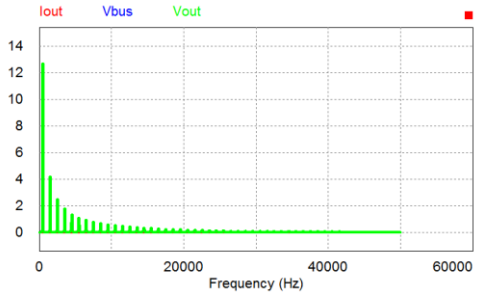

Fig5.5 FFT of a square control signal

Harmonics close to the fundamental are not desired, and that is what is got if control system works with PWM signals: harmonic content close to the fundamental frequency is highly reduced. There are two control strategies based on PWM: Bipolar and Unipolar.

Bipolar Modulation

Working with bipolar modulation output can take two values: +VDC and –VDC. But this time with variable duty, function of the target sine wave to be generated. Next figures Fig5.6 and Fig5.7 shows output signals (voltage and current) and harmonic content respectively. As it can be appreciated, output voltage takes positive values when current must be negative and vice versa. Working in this way THD is 1.04 for the output voltage like in Fig5.6.

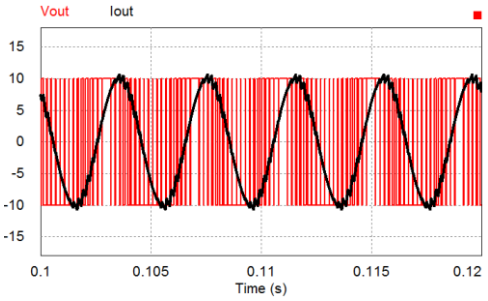

Fig5.6. Bipolar modulation for H-bridge control

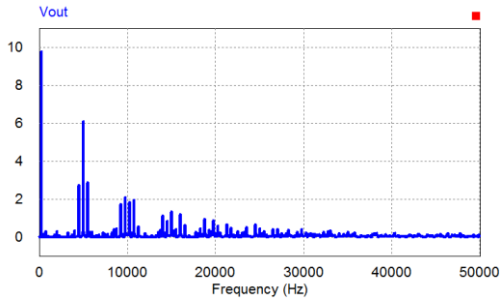

Fig5.7 FFT of a bipolar control signal

Unipolar modulation

Unipolar modulation is the control strategy for an H-bridge with lower THD, because there is not negative voltage applied to the load when current is positive (with resistive load). For the same values of DC bus and references as in the case above, THD is reduced to 0.56 for output voltage. Next figures show output signals when control is performed with unipolar modulation. Note that phase shift appreciated on Fig5.8, is due to the inductive load.

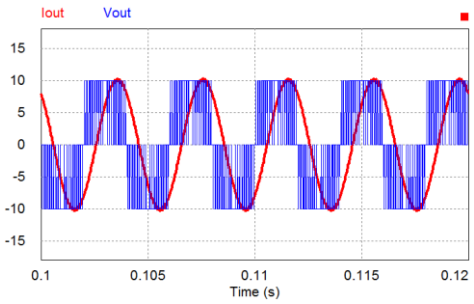

Fig5.8. Unipolar modulation for H-bridge control

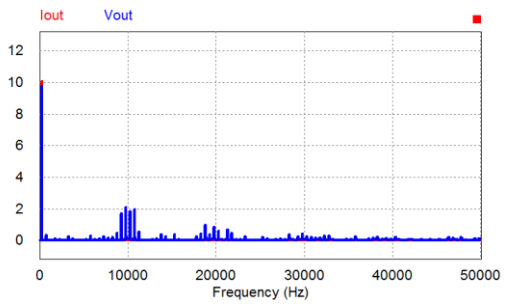

Fig5.9 FFT of a unipolar control signal

4.4. Implementation of bipolar modulation in c code

The DSC selected to control the H-bridge integrates a PWM peripheral, designed to easily control inverters. A counter increases with every internal clock period and another register is set to be compared. When they match, AD interrupt is triggered what means that a PWM period has completed. At this point duty for next period must be set.

In order to generate a sine wave at the output the duty value must be calculated on each AD interruption. Once AD interruption starts, program must know the frequency signal to be generated and the time vector. Frequency is fixed and time is increased on every interruption until complete the period, then time is reset to zero. Actually, time cannot be reset to zero because errors wold be accumulated, a period (2π) is subtracted instead.

Finally, to implement unipolar modulation sine wave references must be complementary, than same as adding a phase shift of 180 degree. Next lines show how duty cycle is calculated for each switching period to produce unipolar modulation on each AD interrupt:

```
#define         f_out    250            //Fundamental output frequency
#define         pi       3.14159165
#define         sw_freq 5000            //Switching frequency
#define         A        65535          //max Amplitude

Void ADC_Interruption(){                //A/D interruption routine
        ADIF=0;                         //Reset interruption flag
        w=2*pi*f_out;                   //pulsation calculation
        t=t+(1/sw_freq);                //increment time count
        PDC1=A*sin(w*t);                //Calculate duty for first branch
        PDC2=A*sin(w*t+pi);             //Calculate duty for second branch
        If(t>=2*pi)
                t=t-2*pi;               //subtract a period if period is completed
}
```

In order to facilitate test and avoid the necessity of having the programmer tool to change amplitude and frequency, an executable program (Fig5.10) was developed and parameteres are sent via UART. It can be executed in any computer with the only requirement of a RS232 port.

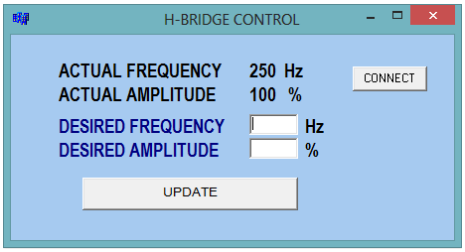

Fig5.10. Control window for H-Bridge

The window showed above indicates actual frequency and amplitude values for the H-bridge output. To change those values integer numbers can be introduced in Edit boxes. Update button send the parameters to the microcontroller and once established in the H-bridge output, microcontroller returns actual amplitude and frequency values to the software.

The PCB built for this task is shown on Fig5.11.

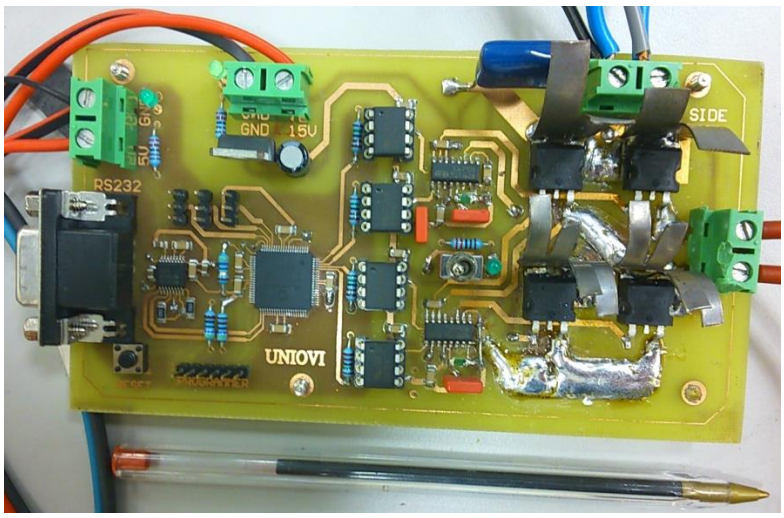

Fig5.11. PCB built to handle the transformer

5. Temperature measurement system

This thesis intends to give some basics on how to measure temperature in a magnet, within a magnetic field variation. There is not information about how sensors and IC's behave in those conditions so that would be another objective of this work. In this section suitable sensors for this application are selected, conditioning system will be explained as well as filtering stages when needed.

5.1. Temperature sensors

Manufacturers offer many types of sensors that can be signal generators, or not; with temperature dependent on resistance or digital, case in which sensor integrated within IC and temperature is read from the microcontroller digitally.

- ***Resistive sensors***: are types of resistors whose resistance varies significantly with temperature. PTC and NTC are discarded, their resistance do not vary linearly with temperature, although NTC can be linearized in a small temperature range. Other resistance dependent sensors are RTD, which varies their resistance linearly with temperature, calibrated to set 100 Ohms at 0 degree. Made of platinum it is a very robust sensor covering a wide temperature range [-200 to 850 °C] and its error can be as low as ±0.03 degree in 1/10B class. It is available in several packages, as small as 0603 standard SMD chip (Fig6.1). It can be found integrated in a thin film (Fig6.2). For this last package, manufacturer warrantees vibration resistance.

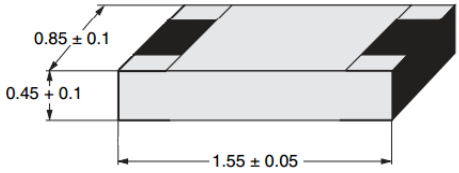

Fig6.1.0603 package of aPT100. Source:Vishay

Fig6.2 PT100 thin film package. Source:RS

Since RTD are usually made of platinum, the relation between temperature and resistance follows the equation (6.1), known as Callendar- Van Dusen equation.

$$R = R_0 * \left(1 + 0.0385 * (T - T_0)\right) \quad (6.1)$$

All features explained above makes RTD sensor appropriate for this application. Further details are explained later.

- ***Thermocouples***: a thermocouple consists of two dissimilar conductors in contact, which produces a voltage when heated. The generated signal is proportional to the temperature difference between the join and the connection point (Fig6.3) known as Seebeck effect. Thermocouples are inexpensive and widely used for measurement and control in industry. Depending on materials, sensitivity change being 41µV/°C for the case of K type. K type is the most common thermocouple, even if sensibility is not the highest, it presents oxidation, vibration and high

temperature resistance. It must be isolated because any new join will alter generated voltage.

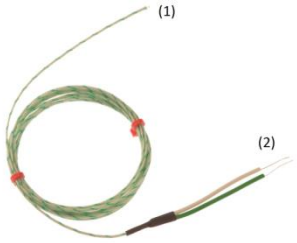

Fig6.3.Thermocouple. (1) Connection side, (2) hot junction

Voltage at its output comes by (6.2), where K is sensibility, V is the generated voltage and T is temperature. To know one of those variables, the rest must be measured what means that temperature at the connection point is needed as well as generated voltage to know temperature at junction point.

$$V = K * \left(T_{join} - T_{connection}\right) \quad (6.2)$$

Here comes its first disadvantage: the need to know the temperature at connection point, besides the accuracy on that measurement is directly reflected on the final data. Since thermocouples are just wires, it is know that a magnetic field variation induces current in the conductors and therefore measurement may increase its uncertainty. Further details are explained later.

- ***Sensors based on diode's knee voltage***: These kinds of sensors work measuring how diode's knee voltage varies with temperature. As it is well known, knee voltage in a diode is affected by just temperature and current passing through. If current is kept constant, knee voltage is therefore proportional to temperature. Commercial sensors like these, integrates the analog to digital converter and all the necessary to send read data through serial I2C.
  All necessary electronics can be found in commercial IC's packages as small as SOT23-6 or SOT563. As advantages, two wires are enough to communicate with up to 127 devices (power wires are required too), apparently they are not affected by magnetic field variations.
  Up to 12 bits resolution from -55 to 150 °C having a resolution of 0.0625°C, ±0.5°C accuracy for −25°C to +85°C (may be reduced by shorten temperature range). The need of adding a capacitor very close to its power pins can make this sensor unsuitable for high temperature applications or may reduce its life expectancy.

- ***Infrared sensors***: Due to its size (see Fig.6.4) infrared sensors were initially discarded. Its principle of operation is based on the measurement of the radiation emitted by the object being measured. The way to get temperature value is by measuring generated current typically.

Fig 6.4. Infrared sensor. Source: New Pyro Couple

Its cost is a disadvantage, as well as the conditioning circuit needed that makes the system worth for few applications only.

5.2. Sensor conditioning

After analysing advantages and disadvantages of the temperature sensors mentioned in the previous section, RTD's, thermocouples and integrated temperature sensors were selected to be tested. All of them present linearity temperature dependence in a reduced size, low cost and although the conditioning system must be built carefully. To adapt voltages between sensors and microcontroller, instrumentation operational amplifiers were used. Their main features are: low offset, low noise, compensated error due to resistance temperature. In addition, for this kind of sensors, input signals must be differential.

5.2.1. RTD's conditioning system

As it was explained above, RTD's are calibrated to set 100 Ω between terminals when temperature is 0 °C having a variation ruled by (6.1). For that, by know the resistance, temperature is indirectly obtained and that is what Wheatstone bridge (Fig6.5) was invented for.

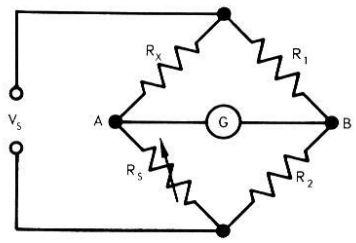

Fig 6.5. Wheatstone bridge

The value of an unknown resistance is measured by adjusting the value of R5. When Galvanometer indicates no current circulating, the relation R1/R2 is the same as Rx/R3. For the PT100 temperature measurement, Wheatstone bridge allows to set zero and gain for the voltage to be proportional to measured temperature.

$$V_{AB} = \frac{R_2}{(R_2 + R_x)(R_5 + R_1)}(R_1 - R_s) * V_s \quad (6.3)$$

Uncertainty Calculation

PT100 temperature measurement system gets imprecise when tolerance of the devices increases. A system like this might be calculated to have certain uncertainty having an idea about the minimum admissible tolerance for each component. For the purpose of this part (measure temperature increments) the uncertainty will be given once system has been built, no special uncertainty is specified.

The equation (6.1) is not linear. When it gets linearized a maximum error must be added to the measurement (6.2). The output voltage of the bridge is amplified with an operational amplifier (OA) what will add a gain error. Finally the offset of the OA cannot be neglected, in fact, is the third parameter that raises uncertainty.

$$E_{max} = E_{gain} + E_{offset} + E_{linearity} \quad (6.4)$$

5.2.2. Thermocouple conditioning system

In the paragraphs above, thermocouple principle of operation was explained: it is classified as a generator signal sensor with linear variation. Concretely it generates voltage. So the aim of the conditioning system is to adapt voltages. Voltage generated by thermocouple is extremely weak so that, the device to be connected must provide very high input impedance, to avoid current circulating; must ensure low input noise, although it could be filtered; and the offset must be close to zero, offset produces a direct error in the measurement. Manufacturers recommend using instrumentation amplifiers (OA) for thermocouples conditioning. The INA 129 is an instrumentation OA that meets all the requirements earlier mentioned, from TI. With very high input impedance and differential input it requires of just an external component to adapt signals: gain resistance. On Fig thermocouple conditioning system is shown.

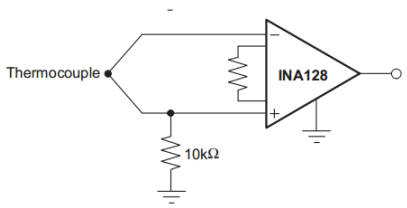

Fig 6.4. Thermocouple conditioning circuit

At this point, signals adaptation is explained, but on (6.2), equation that rules thermocouples behaviour, clearly that is not enough. Temperature at the connection point must be a known value while the voltage generated is proportional to the

difference between junction and connection temperatures. The way to warrantee stable temperature at connection point is by using isothermal connectors, usually sold with thermocouples and sometimes integrates another temperature sensor: RTD or NTC typically. In this project isothermal junction have not been used and temperature IC's are responsible to know connection temperature. The fact of having the measurement system working at ambient temperature, not exposed to sharp temperature changes, justified the technique.

Uncertainty calculation

The uncertainty in temperature measurement is given by the devices needed to signal conditioning and temperature measurement at junction point. When measuring high temperatures, uncertainty of the measurement in the junction point does not have much importance. But for this particular case, measurements of the temperature at junction point are very important since temperature to be measured is quite close to ambient temperature. For that reason, uncertainty in the measurement comes given by (6.5). The OA's offset increases the uncertainty as well as the linearity error (that can be neglected for small measurement ranges).

$$E_{max} = E_{offset} + E_{junction} \tag{6.5}$$

On Fig6.5 It can be appreciated that linearity error increases in the measurement when all measurement range is considered. In the other hand, once range has been reduced linearity error is unappreciable (Fig 6.6).

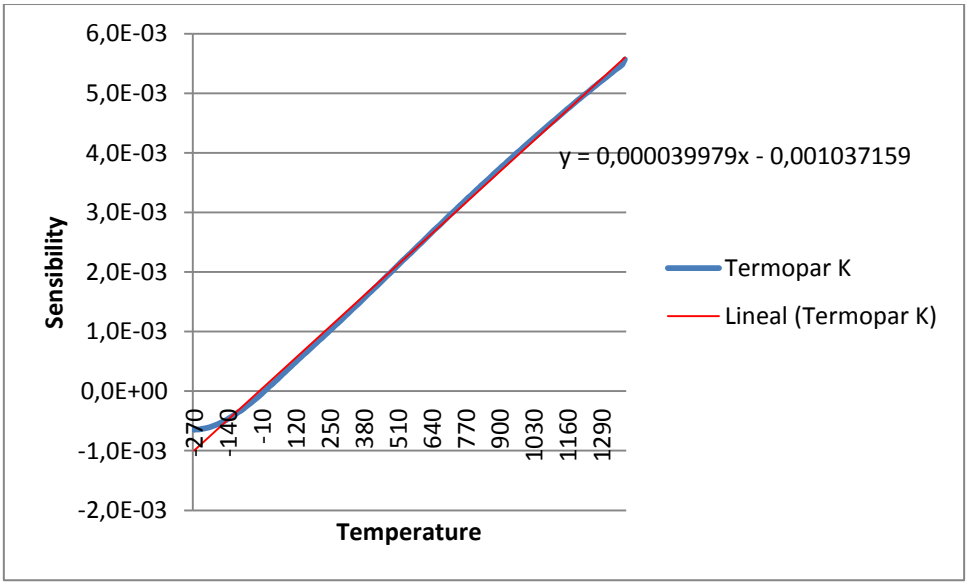

Fig6.5. K-type thermocouple linearization [-270-1370]°C

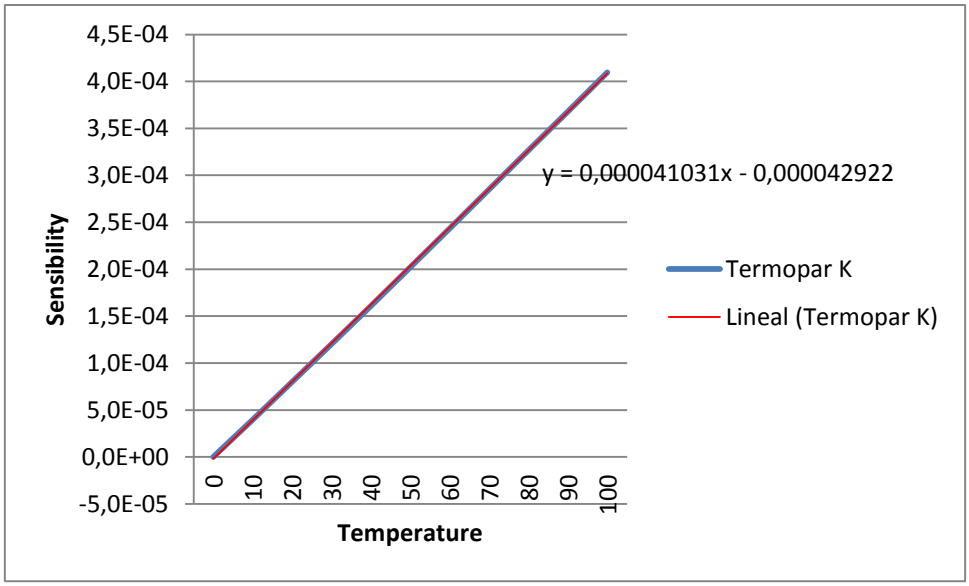

Fig6.6. K-type thermocouple linearization [0-100]°C

5.2.3. Integrated sensors conditioning system

Most of integrated temperature sensors integrate a serial interface to communicate digitally with a master, which handle bus information. To get temperature at the IC's environment, device must be feed, connected to the bus and configured. The IC selected for this test is the TMP100 from Texas Instruments that integrates all electronics in a SOT-23 chip, showed on Fig6.7.

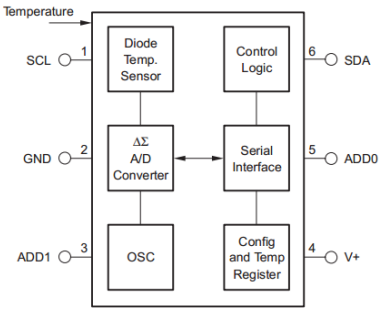

Fig6.7. TMP100 I2C temperature sensor from Texas Instruments

TMP100 can measure temperature in a range of -55 to 125°C with an accuracy of ±3°C. This uncertainty may be reduced up to ±0.5 in the range of -25°C to 85°C. Its 12 bits AD converter provides a resolution of 0.0625°C with a conversion time of 320ms. Conversion time is reduced when resolution or the number of bits set are reduced. TMP100 is also a low power device that requires 40 µA working, 0.1 µA in standby mode.

To differentiate sensors in the bus ADDx pins are set to zero, one or floating, assigning a physical direction to each device. In TMP100, I2C protocol is the serial interface protocol, being able to work at high I2C speeds, up to 3.4 MHz. Since the device has other features, configuration is required to read temperature. Configuration status is saved in a RAM memory what makes necessary executing configuration steps on every power up. For the case of TMP100 configuration algorithm is the shown on (Fig6.8), blue boxes represents slave writing and black represents data sent by the master. First data byte to send represents the address of the device to communicate, where first four bits (•) are set internally by the manufacturer, next tree (•) are dependent on external ADD pins and last one (•) says de device read (1) or write (0). Second bytes onwards are configuration data. The algorithm needed to read temperature is shown on Fig6.9.

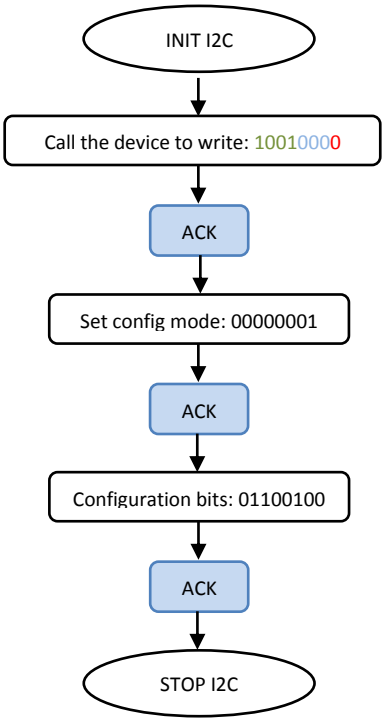

Fig6.8. Flow chart writing devices RAM memory

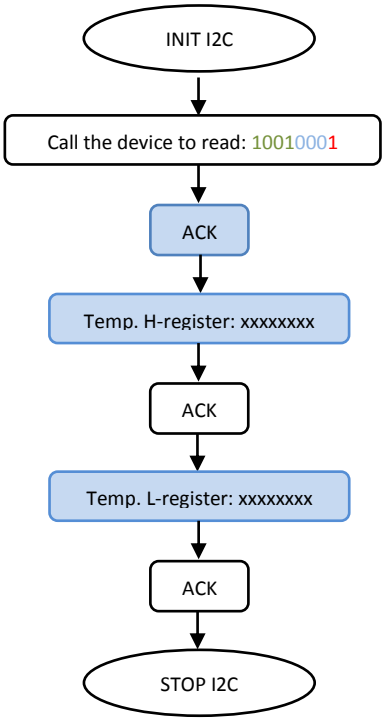

Fig6.9. Flow chart reading temperature

5.3.Filtering stage

When measuring temperature using thermocouples a filtering stage is recommended [11]. Even more, when AC signals are not desired due to radiation or induction phenomena. To know the cut-off frequency for the filter, frequencies that the sensor is exposed, must be known. Transformer is fed by a PWM inverter and its high inductive impedance will filter high frequency signals, so current takes the waveform of the fundamental frequency. Besides, magnetic field is proportional to the frequency and responsible at the same time of the signals induced in the sensor. Therefore, fundamental frequency of the PWM is the target frequency to be eliminated. As temperature varies very slowly, the filter to be

designed will set the cut-off frequency in 1 Hz, being order two. The minimum frequency to test in the transformer is 100Hz where almost 80dB attenuation is warranted with the specifications mentioned.

Filter is calculated with *FilterPro* software, selecting SallenKey topology and Bessel function. Gain is also set to 1 and the results are shown on Fig6.10.

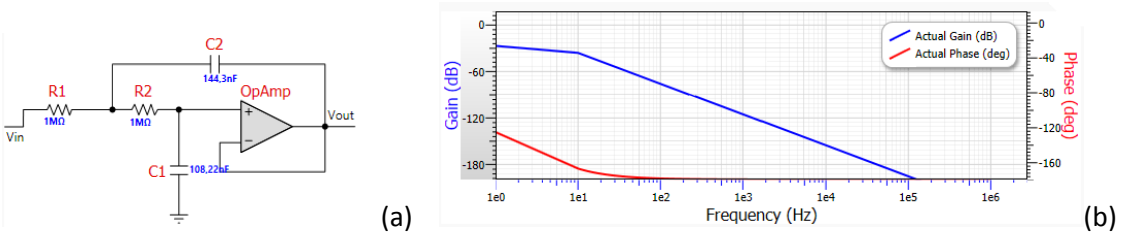

Fig6.10. (a) Sallen Key topology for filter design, (b)Bode diagram of the filter designed.

The operational amplifier used in the filter may be a general purpose operational amplifier. Weak signals were amplified so their offsets have not the important as in the previous stage.

For the case PT100, same principle is applied. Two wires within magnetic field variations are susceptible to be affected. Having the same frequencies in the transformer filtering stage have to work in the same way, adding no offset.

5.4. The AD conversion

Before encountering the analog to digital converter, the input signal is processed with an electronic low-pass filter to remove all frequencies above the Nyquist Frequency (one half the sampling rate) [12]. This is done to prevent aliasing during sampling and is therefore called antialiasing filter.

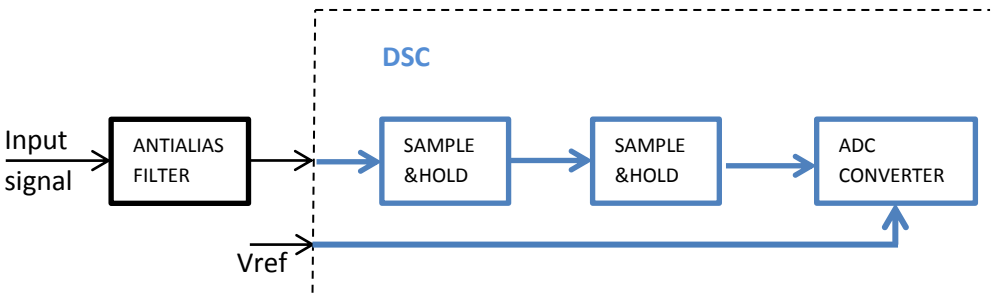

Fig6.11. Block diagram of the AD integrated peripheral in the DSC

Microcontroller integrates a 10 bits A/D converter peripheral (Fig6.11) that will add uncertainty to the total measurement system, mainly due to two reasons: the voltage reference and the resolution.

The AD conversion in dsPIC30F6010A is done by continuously comparing the analog signal with a reference. If the reference is not stable, the conversion will come with errors. To solve this problem, stable voltage references must be used and a good example is the LM4040 from TI that keeps between its pins 4.096, 2.048 or 1.024 volts depends on the model. Those values are not random, they are powers of two in order to give integer values as a result of the conversion. Although it is less common and sometimes not needed, negative reference can be other external input.

The reference used for this circuit is LM4040-4 that sets 4.096v. To calculate the circuit shown on Fig6.12, manufacturer establishes a maximum forward current in 10mA as well as the minimum necessary to work: 68uA.

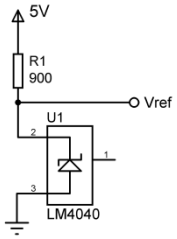

Fig6.12. Circuit needed to get stable voltage reference for the AD conversion

The Vref pin in the DSC is a high impedance input and therefore there will not be current circulating though it. In order to reduce consumptions, current is set in 1mA and the additional resistance is calculated in (6.6).

$$R = \frac{5\,V - 4.096\,V}{1 * 10^{-3}} = 904\,\Omega \qquad (6.6)$$

5.5.Sensor attachment system

The way to attach the different sensors to the magnet may affect the obtained results, having an added error to the calculated uncertainty. When using thermocouples the electrical isolation between magnets and sensors cannot be ignored, any new metal join in the thermocouple will disturb the measurement process. When testing thermocouples in magnet temperatures sensing, insulating tape is enough to warrantee non-contact (Fig6.13). Silicone is typically used to isolate and ensure heat transfer but in this case, same temperature was read with IR thermometer and thermocouples attached using just insulated tape.

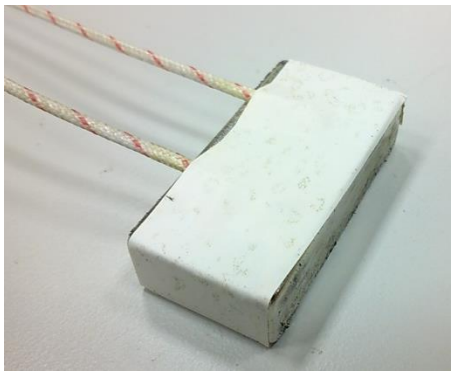

Fig6.13.Thermocouples attached to the magnet

In the case of using PT100 or integrated sensors, due to their size, a solid base is needed. In both cases the solution was to insert sensors in a PCB to reduce air gap in the transformer. The designed PCB can be checked on PLANOS, and the final result in figure below (Fig6.13). These PCBs were designed with very thin tracks (10 mils width), small loops,to reduce current induced by the magnetic field variations since their aim is to conduct signals and there is not power passing through. Fortunately, induced current will not have effect over the final results because it is easily filtered. The interesting signals can be considered continuous while all the AC components are not desired and therefore eliminated.

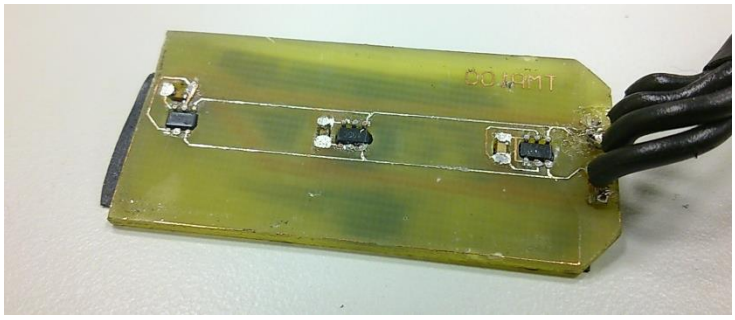

Fig6.14. I2C sensors inserted in a PCB

Fig6.15. I2C sensor card between two magnets

To ensure thermal conduction in this case, thermal paste can be used as well as insulation tape to avoid non desired electrical contacts. Details in the final view can be checked on Fig6.16:

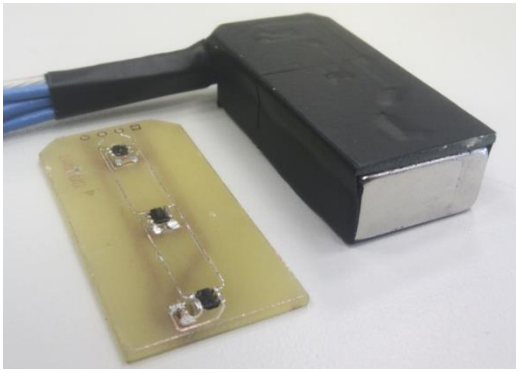

Fig6.15. I2C sensor card and magnet with PT100 card attached

5.6.Prototype design

Although this prototype is designed to be tested in a modified transformer, a similar system will be installed within an electric motor where electronics have to be as compressed as possible. The prototype must easily allow changing the communication interface (see Fig6.16 and 6.17) to evaluate how communication systems are affected by strong magnetic fields variations. To avoid problems of electro-magnetic compatibility (EMC), basic rules of PCB design [11] were followed.

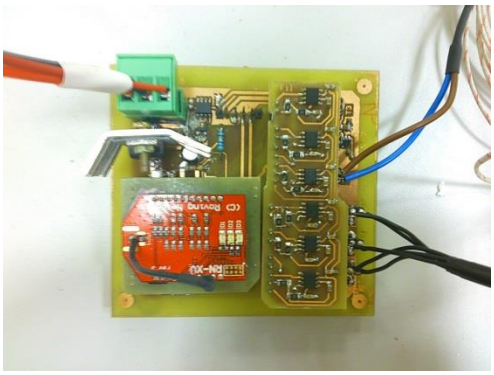

Fig6.16. communication via Wi-Fi

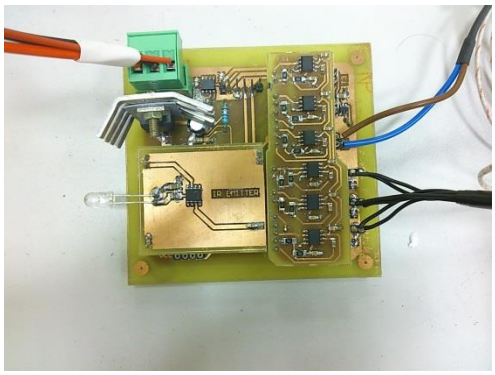

Fig6.17. communication via Infra red

To minimize wires length in the PCB, three single PCB were built. First in the base, second the filter stage (that can be removed), and third the PCB that holds the different communication cards: Wi-Fi, RS232 and IR. Fig 6.18 and Fig6.19 show it.

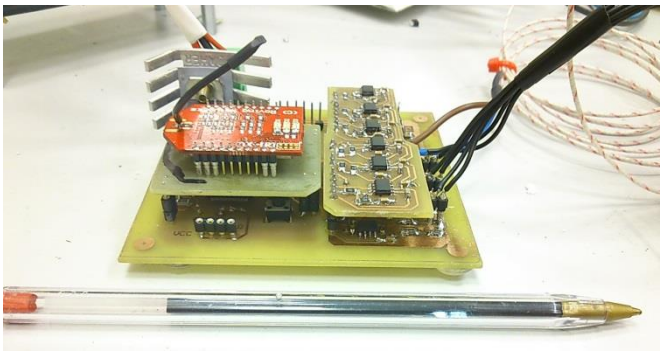

Fig6.18. Board containing conditioning, filtering stage, DSC and communication system

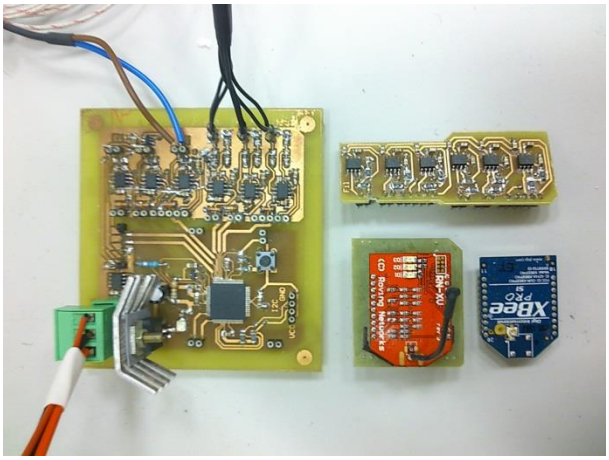

Fig6.19. Different PCB of the measurement system

With this design all possible communication system can be tested by just removing the card and plugging a different one. Removable filtering stage allows to test if a filter stage is need.

6. Communication system

The objective of this project is not only to evaluate how magnets temperature varies when high frequency signals are injected, but also how the system can be attached to an electric motor to monitor rotor temperatures and know how data can be extracted. Rotor will be turning and data must be extracted to verify magnets temperature estimation methods in explained in [6]. The aim is to receive in a PC all data sensed in the rotor while turning. The methods explained below are proposed and successfully tested in the lab. In the other hand, the possibility for the system to be auto-feed is evaluated as the access to magnetic field variations is direct. In this work several wireless technologies are tested: Infrared, Zig-Bee and Wi-Fi modules. Some others were discarded. Bluetooth modules for instance, require higher power than Wi-Fi or Zig-Bee in active state. Or low frequency radio communication that may have higher vulnerability to electromagnetic fields.

For testing the transformer, the hardware was designed to evaluate all the systems with the possibility to choose the communication system at any moment. Standard PCBs were built to easily interchange the different technologies during the process.

6.1.Communication speed calculation

Temperature dynamics is very slow which allows the communication system to work at very low speeds. In the case of working with the motor up to 16 sensors can be read with 12 bits resolution by the DSC, data to send via asynchronous bus UART (8 bits). To recognise one data byte in the bus, start and stop bits are used, so for every byte transmitted 10 bits are sent (Fig7.1).

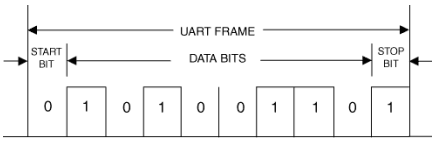

Fig7.1. UART data bits

To identify where the first sensor is placed, 8 bits header is added the message. Two bytes per sensor 16 times plus header makes a total of 330bits to be transmitted every sample. A proper time interval to evaluate temperature changes in a motor could be 5 minutes but this value cannot be used to calculate baud rate because transmitter modules would be active for long time, wasting energy. Transmission time is set in 50ms. Minimum allowed baud rate to respect times is therefore (7.1), but choosing a common baud rate, total transmission time is (7.2),

$$baud\ rate(min) = \frac{330}{0.05} = 6600\ bps \tag{7.1}$$

$$transmission\ time = \frac{330bits}{9600} = 0.034\ s \tag{7.2}$$

6.2.Communication using IR transceivers

Infrared (IR) communication is a widely used wireless technology, communications system can be built with quite simple electronics with low cost devices when the rate speed

is not too high. Besides, infrared light works in a non-visible environment with a wavelength from 700 nm to 1 mm being 900 nm a typical value for IR emitter diodes.

The Idea is to install the IR emitter in the shaft centre having a few centimetres detached receptor, as Fig7.2 shows. In those conditions, measurement system will be turning with the rotor but from the point of view of the receptor, the IR emitter will be motionless. Note that polarized used sometimes to reject disturbances cannot be used since emitter turns at variable speed.

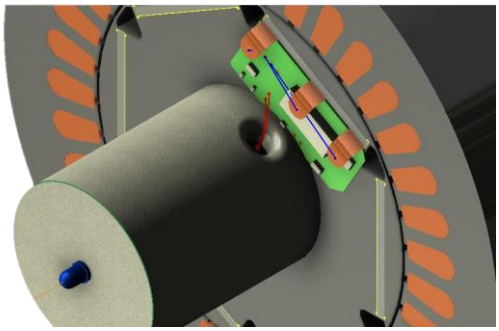

Fig7.2. IR emitter installed in the rotor

The hardware needed to carry out a wireless communication is shown in document two (see PCB and schematic index pag51), but to understand the necessary stages, see Fig7.3.

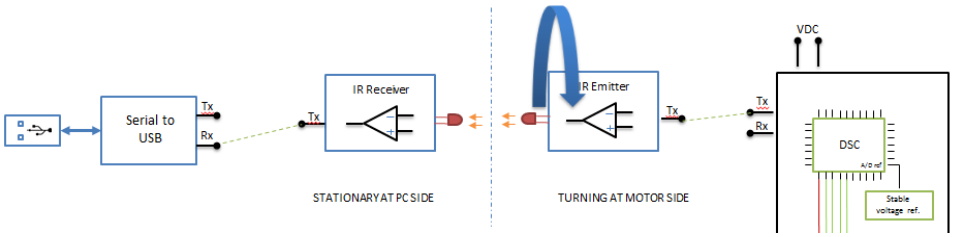

Fig7.3. Block diagram of the IR communication

For the laboratory test, data sent through IR uses RS232 data form. In order to standardize the acquired data, IrDA protocol should be implemented, to facilitate the received data to be read with any IrDA commercial device and reject interferences. The DSC mentioned above, integrates the IrDA peripheral.

The minimum hardware needed to carry out this communication is summarized on Fig7.3 and explained below:

Hardware at DSC side

The IR emitter could be directly connected to the DSC pin to 5 volts because the microcontroller is able to deliver 20 mA per pin, being that a typical value for the forward current in common IR emitters. But an operational amplifier connected as emitter follower is used, to reduce the demanded current.

To select proper components rated work speeds must be known, being 256 Kbps the maximum speed the DSC is able to work with. But for temperature applications, 256Kbps are wasted while it varies slowly. For this application 9600 Bps was set, microcontroller can works at less frequency reducing also energy consumption and most of the general purpose operational amplifiers in the market allows that frequency to pass through without attenuation. Same for the case of the IR emitters, where cut-off frequency is typically located in tens of MHz

Total current consumption for the circuit is very less, 20 µA for the case of the operational amplifier chosen (MCP6231) and around 20mA while transmitting which make this system suitable for battery supply.

Hardware at PC side

The sensing device to detect IR pulses is the photodiode that generates a current or voltage when IR light is detected. It works therefore as a current generator or as a voltage generator being the first the recommended way to work in communication systems [11]. With an operational amplifier connected as a transimpedance amplifier (Fig7.4), current is converted to voltage, and its output can be now the input of the USB interface.

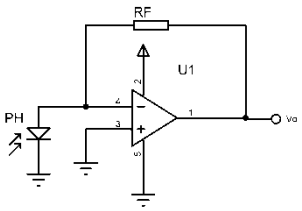

Fig7.4. Transimpedance amplifier for current to voltage conversion

The transimpedace circuit, due to the photodiodes physical characteristics, may become unstable at certain frequency [11], because a zero is added to the system (see Fig7.5) at the frequency (7.3). It can be compensated by adding a capacitor with value(7.4) in parallel with the feedback resistance, calculated by knowing the parasitic capacitance of the photodiode.

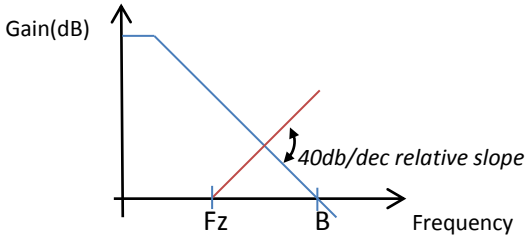

Fig7.5. Open loop bode of the transimpedance circuit

In the figure above, the bandwidth (B) is limited by the circuit. In this case, limited by the Operational Amplifier MCP6231 set in 300KHz. Parasitic capacitance value of the photodiode used BPW34 is 70pF and finally the feedback resistance was set in 100 KΩ. because having 0.05mA of maximum light current the amplified voltage will be 5 volts.

$$Fz = \frac{1}{2 * pi * R_f * C_d} \tag{7.3}$$

$$C_{min} = \frac{1}{4\pi * Rf * B}(1 + \sqrt{1 + 8\pi Rf * Cf * B} = 346\, pF \tag{7.4}$$

Finally, frequency response of the circuit after zero compensation is shown in Fig7.6 and f1 and f2 are calculated on (7.5) and (7.6) respectively. Now receptor system is stable in frequency. Compensation capacitor chosen was 1nF.

$$f_1 = \frac{1}{2 \cdot \pi \cdot 100k \cdot (70 \cdot 10^{-12} + 1 \cdot 10^{-9})} = 22{,}5\ Hz \tag{7.5}$$

$$f_2 = \frac{1}{2 \cdot \pi \cdot 100k \cdot 1 \cdot 10^{-9}} = 1591\ Hz \tag{7.6}$$

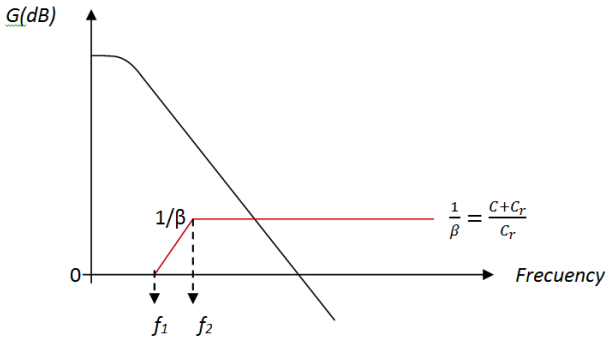

Fig 7.6. Open loop gain and parasitic capacitance compensation

Data is read in the PC through USB port since modern PCs does not integrate RS232 port, so it must be adapted from UART to USB. The easiest way to do it is by creating a virtual COM port in the PC adding a FTDI chip between USB and UART. Connection schematics can be checked in document three (see index of schematics and PCB).

6.3.Communication using Zig-bee modules

ZigBee is a specification for a suite of high level communication protocols used to create personal area networks built from small, low-power digital radios. ZigBee is based on an IEEE 802 standard. With a low power consumption devices often transmit data

within 100 meters radio that can increase adding intermediate devices. X-bee modules are manufactured by Digi International, with reduced size and low cost. It may work in several ways but for this application we are interested on transmitting UART data point to point. Modules are configured by software with X-CTU interface. At the end data send to the device via UART is transmitted to the other point and can be read in the same way Fig7.7.

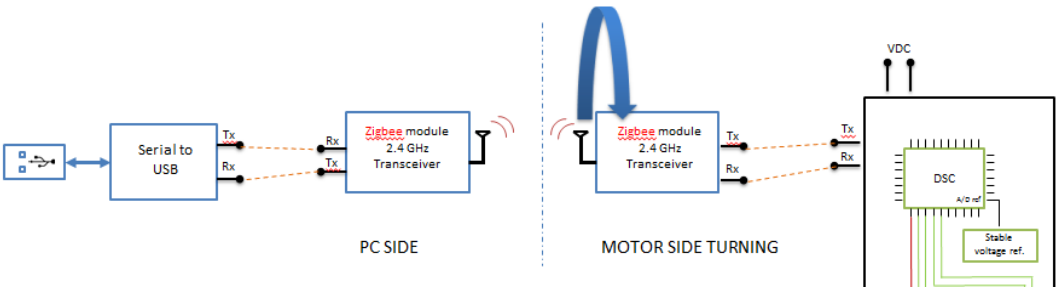

Fig 7.7. Block diagram of the Zig-bee communication

Modules integrate an omnidirectional antenna what allows to turn without affecting the communications. For the case of the motor there will be one transceiver turning attached to the shaft, sending the read data from the DSP. At the PC side, other X-bee module will receive the data and as in the case before, FTDI chip is used to read data from PC.

6.4.Communication using Wi-Fi module

In recent years communication systems based on standard Wi-Fi have been enhanced in features and cost. Roving Networks developed a Wi-Fi module with the same principle of work as X-bee modules: the input UART signals are transmitted via wireless but this time using 802.11 b/g protocol, low cost and easy to program. The advantage now is that most of actual PCs integrate a Wi-Fi card so just one transceiver is required to close a communication environment. The connection block diagram is shown on Fig7.8, being the PC Wi-Fi card the transceiver at the PC side.

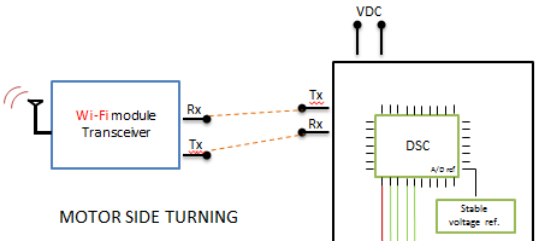

Fig 7.8. Block diagram of the Zig-bee communication

To build the hardware, the only thing to take into account is that the module works at 3.3 volt so signals must be adapted.

Software configuration

The RN171 has basically two ways to work: it can create an access point or it can work associated to an available access point. The second one is the chosen in order to reduce power consumptions, the module will connect to an access point, will send the data to finally switch to sleep mode where consumption is reduced to 1μA.

To configure the RN171, PC can be used, as well as any device able to send data via UART. Once configured, data is saved in a flash memory, what warrantees data availability after power disconnection. At least, the following features must be configured:

- SSID of the access point
- Channel
- Authentication form
- Connexion mode
- Passphrase
- IP of the remote server
- Port of the remote server

Other configuration is required to say the device the working modes that includes: sleep and awake time, connection mode, buffer state, alerts… Some pines facilitated may be configured to force the device to connect, to sleep or as indicators of connection status. This would be other valid way to work, forcing the device to work from the microcontroller. In any case, data bytes are enclosed in packets and sent when a packet is completed.

6.5.Monitoring Software

In the sections above the way to convert the variable to measure, temperature in this case, and send information to a PC was explained. At this point, software is needed to visualize, save or evaluate the information. Borland C++ Builder is a rapid application development environment (RAD) owned by Embarcadero Technologies. Taking advantage of this tool, executable applications can be easily build in this case to read serial ports, information coming from a client and data representation.

Next figure shows the software developed to convert data in graphics, with the possibility to save in excel or txt both temperature and acquisition times.

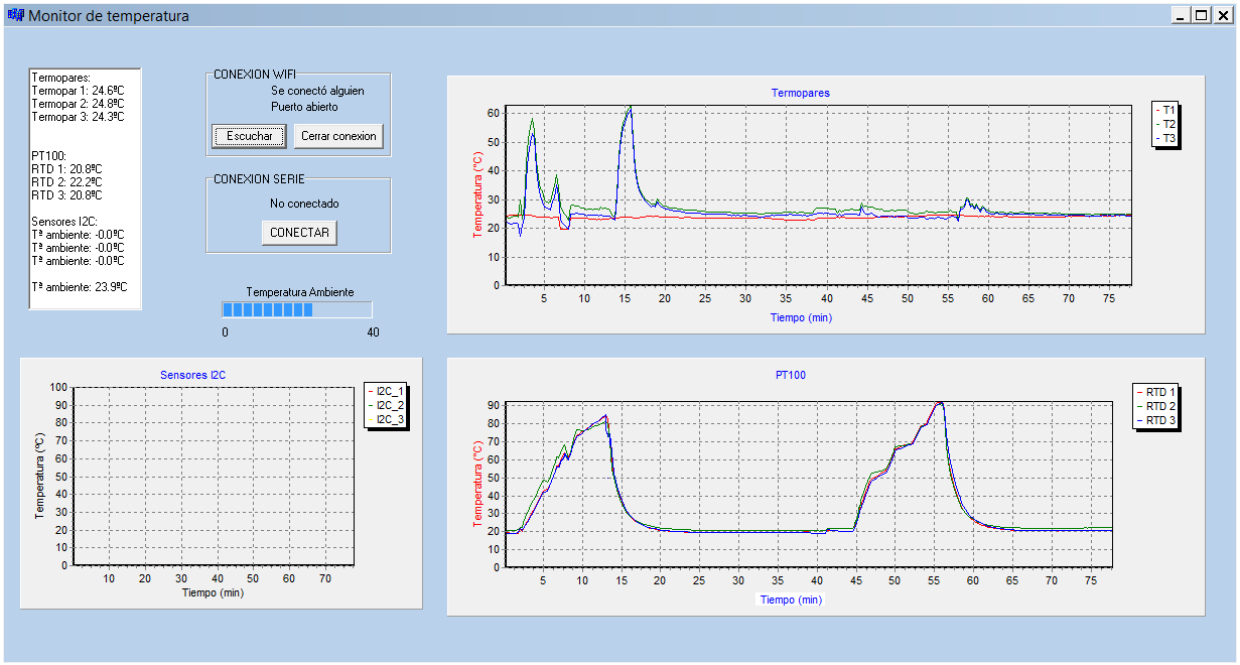

Fig 7.9. Window designed to monitor temperature

Connection via Wi-Fi module

When this kind of connection is used, serial connection is not allowed and automatically disabled. Graphs and rest as well as the rest of information is updated when the client writes and generates an event. On that point, received data is saved, converted to float values to be finally displayed. Vector time is also updated to show a reference time.

Connection via Serial Port

Using serial communication the Wi-Fi menu is disabled. Once connection button is pushed data

7. Simulations

Before building the prototype, some simulations were done with Finite Element Analysis (FEA) software, specific for electrical devices design: JMAG-Designer. The software allows simulating 2D and 3D models in which the following analysis can be executed:

- Magnetic field analysis: eddy current loss in laminated steel, harmonic current input or magnetostriction analysis. Static, transient or frequency analysis can be executed.
- Structural analysis: piezoelectric analysis. Static, transient or frequency analysis can be executed for this case
- Axisymmetric analysis: Static, transient or frequency analysis can be executed for this case

7.1.E core transformer simulations

The modified transformer model was created in 2D taking advance of the JMAG integrated CAD software. After set materials for each part, a mesh that will establish the detail level for each area, was created as shown in Fig9.1. Small areas are defined on the magnet and on the adjacent parts. This will allow to reduce the calculation time, keeping high detail level on the interested areas.

After CAD model creation, materials must be added to each component and also the conditions, in this case, FEM direction in the coil and symmetry boundary.

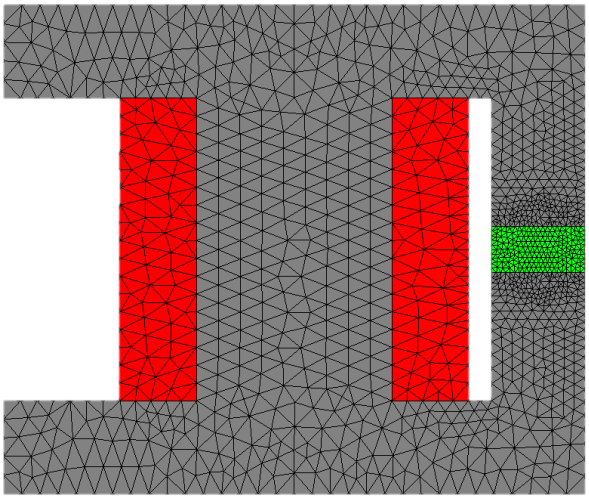

Fig8.1. 2D finite element division of the modified transformer

Finally the electric circuit is linked to the CAD model and power source defined. For the simulations, the source will be a voltage sine wave generator with 20 V amplitude and 250Hz frequency. The only variation in the system will be magnet temperature from 20 to 140 °C.

Feeding the transformer with the voltage waveform set above for all cases, current varies by just changing the temperature of the magnet. This means that the magnet resistance is been increased while magnet temperature increases.

By applying fast Fourier transformer to the resulting data, harmonics at fundamental frequency (250Hz) are obtained, with its corresponding phase shift what allows getting the total impedance. The real part of the total impedance represents therefore the Total resistance of the transformer. Table 8.1 summarizes the results for each case.

Table8.1. Total resistance calculation

Magnet Temp.	Voltage	Current	Impedance	Resistance
20°C	0.00 -20.00i	-0.66 - 0.359i	12.61 +23.30i	12.6168
60°C	0.00 -20.00i	-0.63 - 0.348i	13.37 +24.27i	13.3772
100°C	0.00 -20.00i	-0.61 - 0.343i	13.70 +24.68i	13.7042
140°C	0.00 -20.00i	-0.61 - 0.341i	13.94 +24.96i	13.9410

Resistance data are represented in Fig 8.3 where a remarkable difference in the resistance shows up just by varying magnet temperature. Note that this simulation does not take into account resistance variation in coil due to Joule effect that in practice will produce an error.

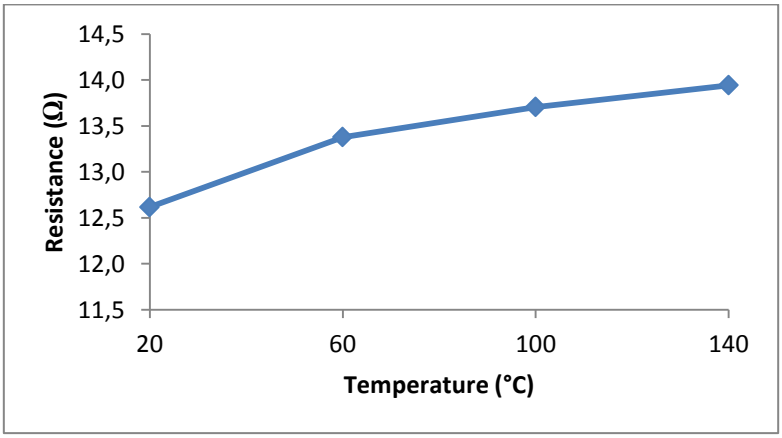

Fig9.3. Total resistance variation with magnet temperature variation

Another powerful tool of JMAG-Designer software is the contour plot. By applying contour plots, visual effects can be added to the model to graphically represent and measure magnetic flux density, magnetic field strength, magnetization, current density…

Magnetic flux density and current density are shown on Fig8.4 and Fig8.5 respectively. Current density in the magnet is higher than in the coil or in the core. Fig9.5 can be also a

mirror of how elements will heat themselves. For instance, coil temperature increases as function of the amount of current passing through it.

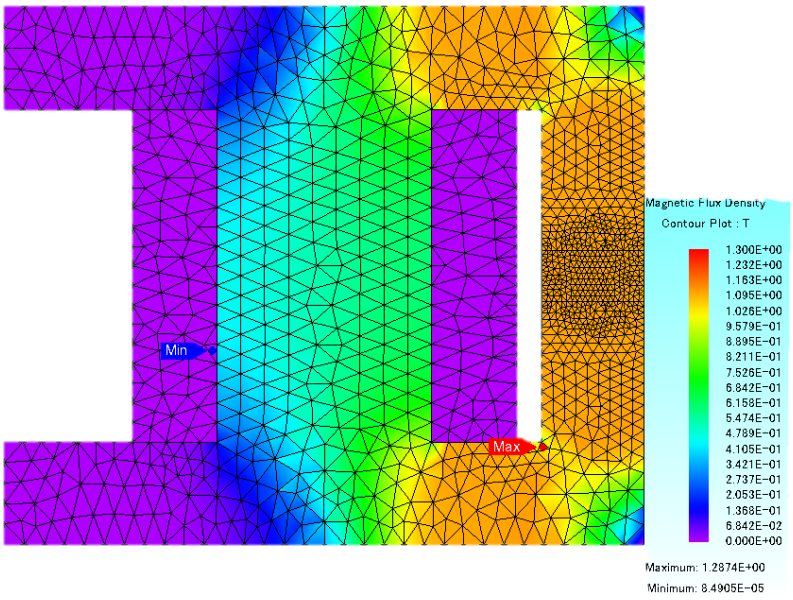

Fig8.4. Magnetic flux density contour plot

Here it can be checked that all the magnetic flux is driven to pass through the magnet creating thus, eddy currents.

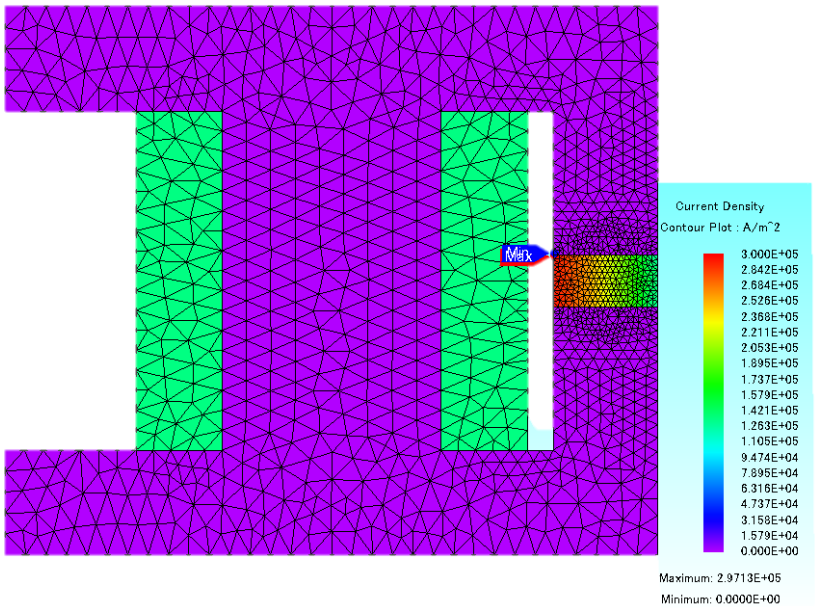

Fig8.5. Current density contour plot

Transformer core was set as laminated so eddy currents are highly reduced. Magnet is a heated by eddy currents because it is a clock, leaving free way for currents to circulate.

But there is a range in frequency, as it will be explained below, for which eddy currents will be high and at the other end, skin effect appears, and eddy currents are lower.

7.2.Toroid core transformer

This transformer was built after checking that it is not possible to appreciate a variation in the magnet resistance when magnet is heated in the case of E core transformer. The magnet resistance portion is very low and any heated radiated to the coil heated it and results got useless. The same happened when core got hot, that resistance was more significant than magnet resistance variation.

This model was built for two reasons: to isolate the coil from the magnet (avoiding heating transference) and due to the way it has to conduct flux. Fig 8.6 shows the real system, where coil is thermally isolated from magnet.

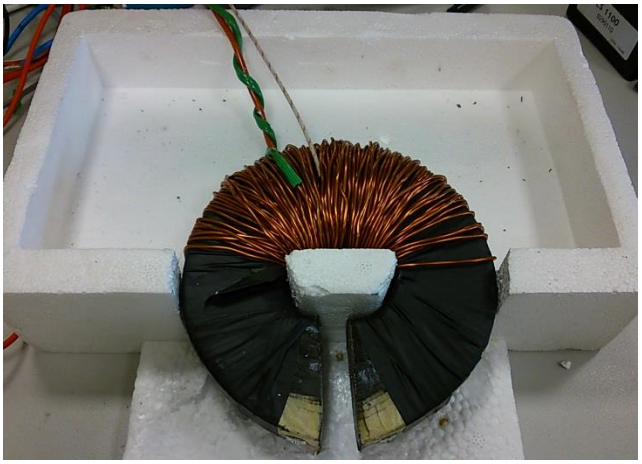

Fig8.6. Real toroid transformer

When simulations were done, Fig8.7 and Fig8.8 were obtained, giving uniformly magnetic flux density distribution and high eddy currents. The equivalent circuit did not change and all measurement system were used in the same way as before.

Results were very different, no temperature variations in the coils and higher magnet resistance. A little variation in core resistance appeared when magnet was inserted hot.

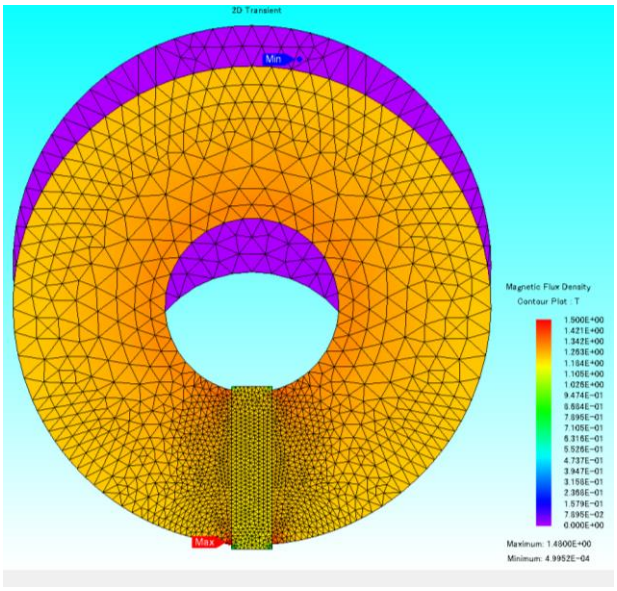

Fig8.7. Magnetic flux density in toroid transformer simulation

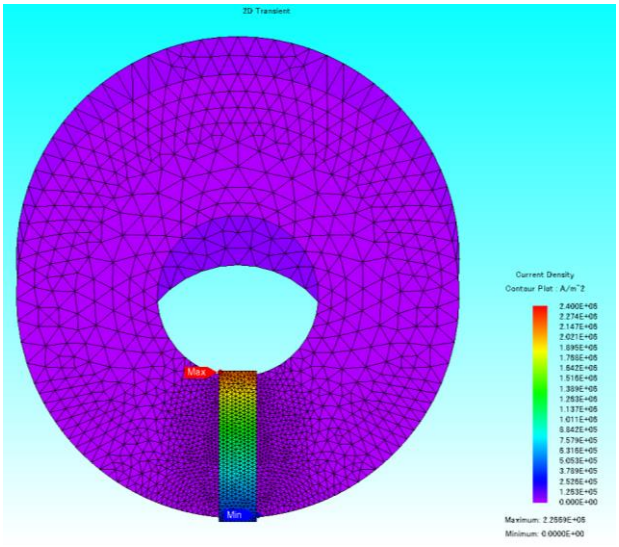

Fig8.8.Current density in toroid transformer simulation

The simulation step showed on Fig8.8 is when current through the coil is zero amps. It can be appreciated that the current density in the magnet at that point is maximum and it is therefore 90 degree shifted respect to current in the coil.

8. Laboratory tests

All theoretical predictions must be done in practice because reality is different than simulation world. First E core transformer will be tested, heating just the magnet and taking measures of impedance for all frequencies, and the magnet will be heated by eddy currents with constant signal injection. Flux weakening and flux intensifying will be apply to the magnet to check what happens.

The objective of the experiments done below is to verify that the method can be physically implemented. When simulating, all the parameters can be easily set but in reality, is very difficult to keep constant parameters that will affect to the final results. For instance, a small variation in the core temperature will affect to the final result and the same happens when winding temperature is not kept constant. That is the reason to use three models, to minimize impedance variation due to unwanted phenomena.

8.1. Transformer with one coil one magnet

First experiments were done with the modified transformer shown on Fig9.1. Its winding is connected to the H-bridge to inject the signal waveforms to be analysed. One thermocouple will monitor winding temperature and three RTD sensors will monitor magnet temperature. At room temperature (20ºC) winding resistance was measured indirectly, due to its small value, with the circuit shown in Fig9.2 and Results are summarized in Table9.1.

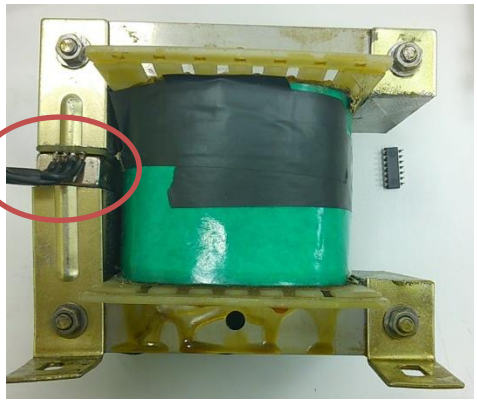

Fig9.1.E core transformer with one magnet

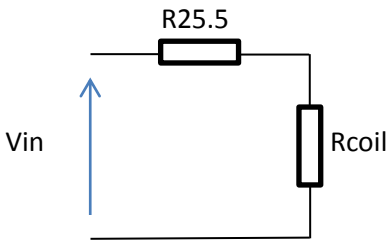

Fig9.2.Circuit needed to measure low resistances

Table9.1. Coil resistance measurement

Vin	Vcoil	Rcoil
1.253	30.3mV	0.6233
1.983	48.1mV	0.6348
2.996	72.6mV	0.6333
4.080	98.8mV	0.6343

From table 9.1 it can be concluded an average coil resistance of 0.6337 ohms at 20°C. First experiments gave a result of around 0.65 ohms working at 100Hz. For t250Hz resistance increases little bit more but still insignificant differences. Besides, almost no difference was appreciated when magnet was heated. The sum of core resistance plus magnet resistance is about 20 mili-ohms what makes impossible to see changes.

With this model several differences were appreciated when the whole transformer was heated at several frequencies but it does not help it was just verified that higher frequencies produce higher magnet temperature at steady state (see Fig9.3). The determinant value to stop studying this model was Fig9.4. Almost the same resistance was obtained with and without magnet in the air-gap.

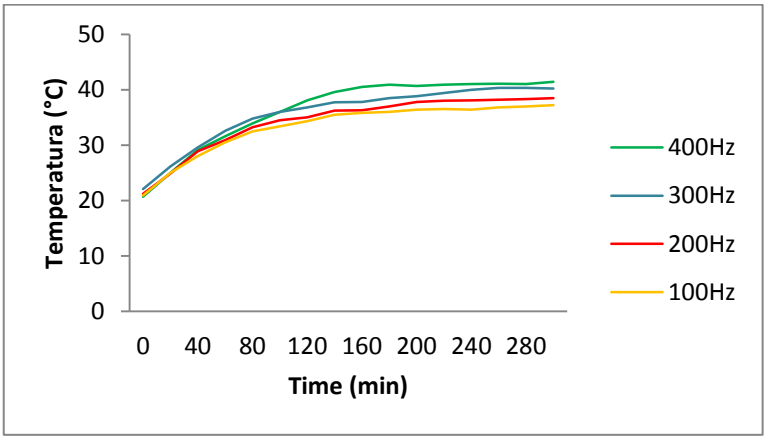

Fig9.3. Transient temperature in the magnet

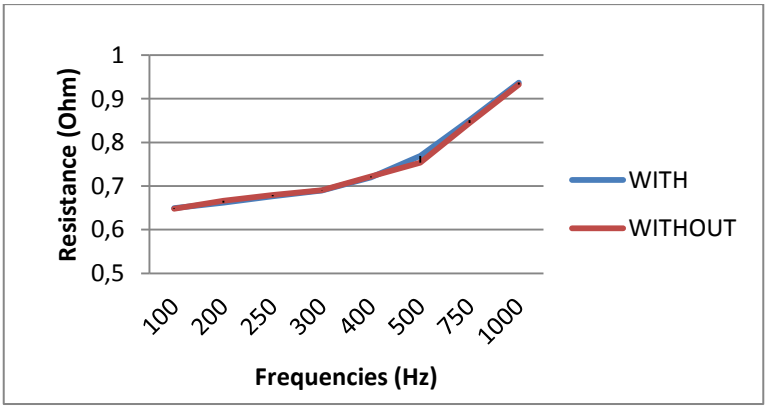

Fig9.4.Resistance read with and without magnet in the air-gap

Next step is to do something to increase magnet resistance proportion in the final value taking advantage of the system already built.

8.2.Transformer with two coils two magnets

The idea to increase the magnet resistance against the total is by double the air-gap size allowing two magnets to fit as in Fig9.3. In addition two coils were series connected to double magnetic field density.

With the same circuit as in Fig9.2, coil resistance was calculated having this time double the value before: 1.2606 Ohm. Same tests are done and same results found: Magnet resistance is still too low in comparison with the total resistance of the system (Fig 9.6).

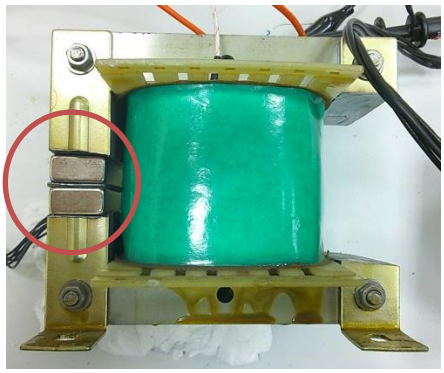

Fig9.5.E core transformer with two magnets

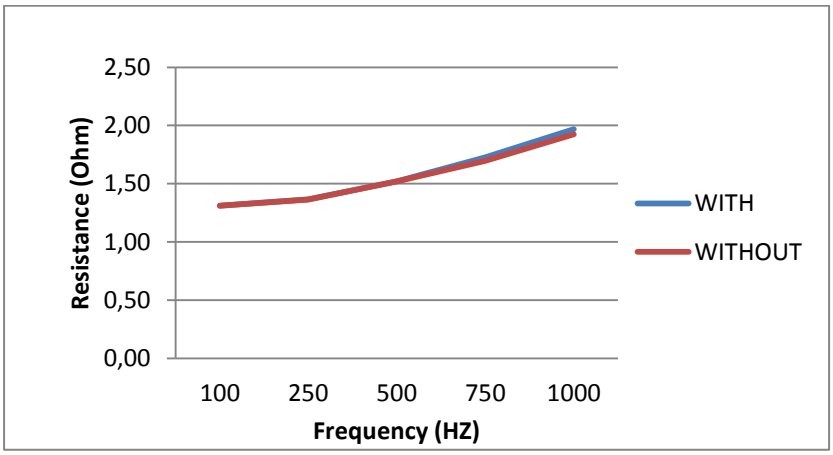

Fig9.6.Resistance read with and without magnet in the air-gap

This experiment cannot be done by using an E core transformer. Other geometry is needed to maximize the effect of the magnet resistance against the coil and core resistances.

Planned system would work only if coil temperature can be kept constant as well as core temperature while heating the magnet. Not physically feasible.

8.3.Toroid core transformer

The main characteristics of this system now are: very low coil resistance, and very low core resistance having a magnet with high importance. The coil resistance now is 0.2381 Ohm, resulting of the average values held in Table9.2 obtained with the same circuit as in the previous cases.

Table9.2. Coil resistance measurement

Vin	Vcoil	Rcoil
1.297	12.3mV	0.2448
2.062	18.7mV	0.2381
3.008	28.0mV	0.2400
4.167	37.7mV	0.2334

Same tests as in the previous cases were done, trying to quantify the value of the total impedance against the magnet impedance. Two tests were done, at 250 and 500 Hz keeping the magnet at ambient temperature (20°C) and obtaining total impedance of the system. The results are shown in the on Fig 9.7. As it can be appreciated, for this geometry the magnet and core resistance represents 65% of the total measurement at 250Hz and 76% when the signal injected turns at 500Hz.

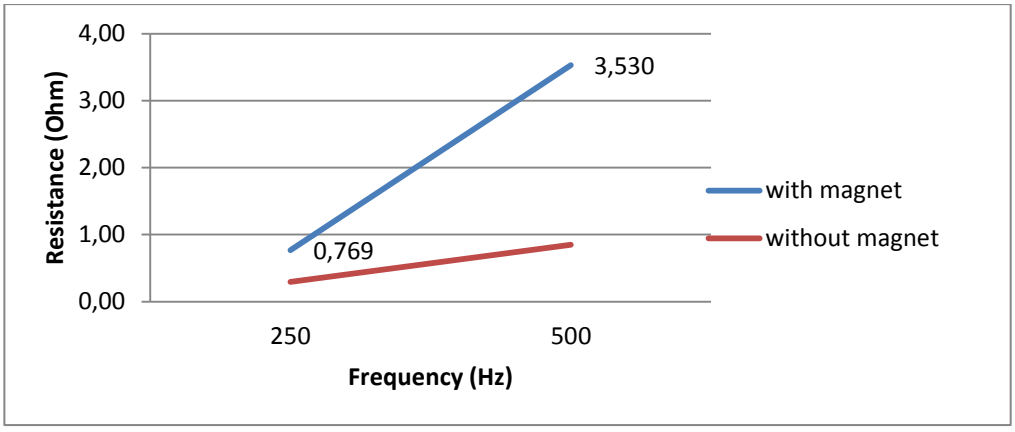

Fig9.7.Resistance read with and without magnet in the air-gap for the toroid

A balance in frequency must be found. It is assumed that core plus magnet resistance is very high this time. Since transformer core is laminated, eddy currents induced on it are assumed very low, but it cannot be forgotten that at high frequencies that currents will take

more importance. At the same time high frequencies will drive to skin effect in the magnet, obtaining false results.

At this point the importance of the magnet resistance in the whole system has been demonstrated. Next tests were done to find out how temperature variations in the magnet can alter total resistance. Magnet is now heated outside the core and introduced for every evaluation. Frequencies of the signals injected were 250Hz (Fig9.8) and 500Hz (Fig9.9). The results are notable variations in the second decimal for the case of 250Hz and variation in the first decimal when the injected signal varies at 500Hz. In the case of working with E core resistance variations were appreciated in milliohms for a the range 80-20°C.

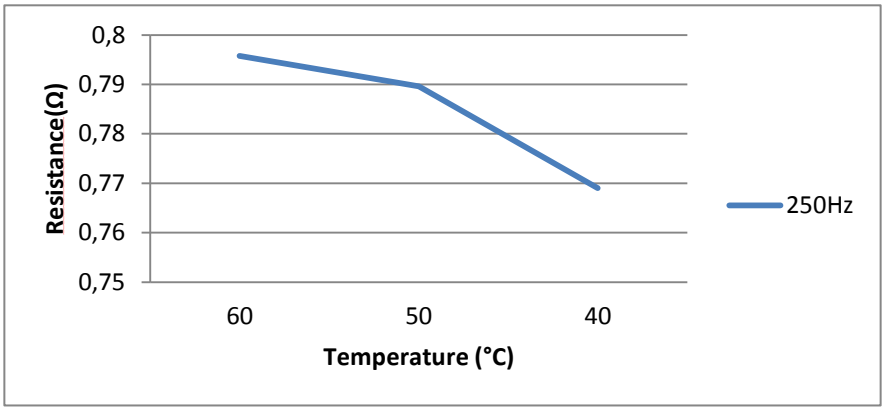

Fig9.8.Resistance read at 250Hz when magnet is heated

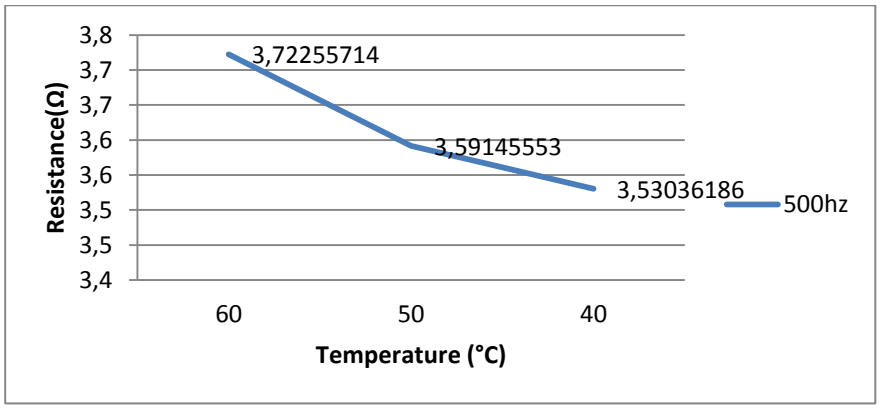

Fig9.9.Resistance read at 500Hz when magnet is heated

Measurements were acquired from 60 to 40ºC because the resistance is sensitive to core temperature variations produced when heat is radiated to transformer core. Figure below (Fig9.10) shows a representation of what happens when a warm magnet is introduced in the air-gap, letting it to get cold at ambient temperature.

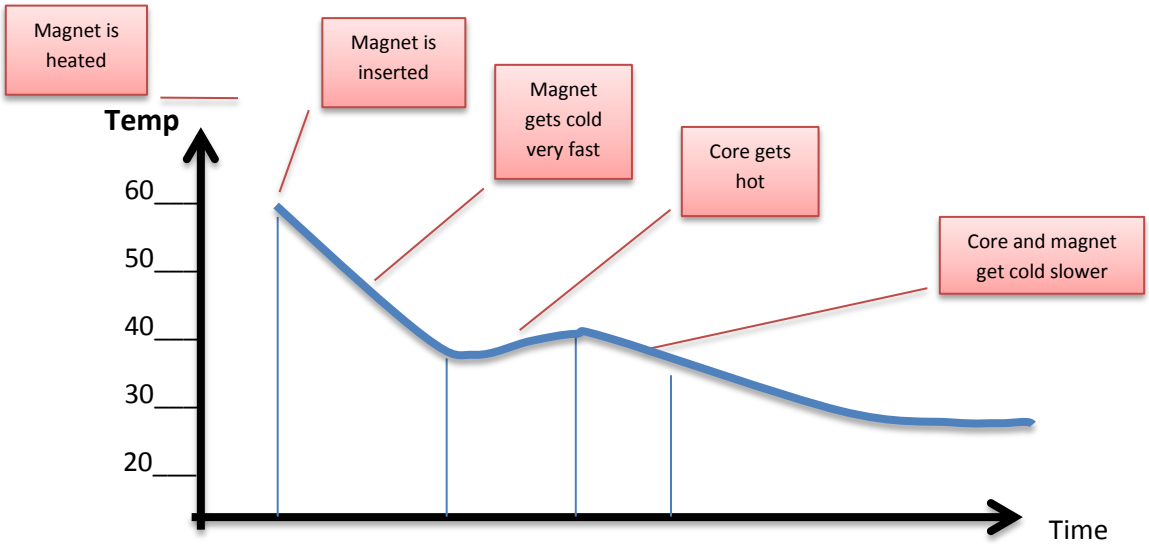

Fig9.10.Resistance read at 500Hz when magnet is heated

For the measurements done above, total resistance is the sum of the coil, core and magnet resistance (9.1). For the case of the low frequency injection (250Hz) the lower losses in the core are assumed due to its lamination and coil resistance temperature was measured during the acquisition time ensuring no variation. So that, with the data obtained in the experiments we can get the magnet temperature coefficient (α) if it is intend to estimate temperature.

Total resistance (Rt) *= Coil resistance (Rp) + Core resistance (Rc) + Magnet Resistance (Rm)* (9.1)

Once magnet temperature coefficient has been obtained (see Fig9.11 and equation (9.2)), magnet temperature can be estimated now as equation (9.3) shows for the case of the lowest resistance obtained taking 60°C resistance as reference. In the equation (9.2) temperature coefficient is obtained by dividing the value from the graph by the resistance at T_0

In this case the chosen reference was at 60 °C.

$$\alpha_{magnet} = \frac{slope\ (graph)}{R_0(T_{60})} = \frac{0.00133}{0.5039} = 0.00264 \qquad (9.2)$$

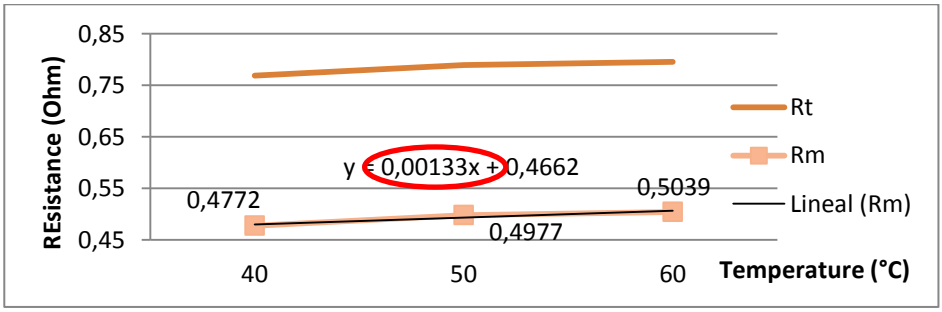

Fig9.11.Manet temperature coefficient calculation

Temperature Calculation

Now, having the magnet temperature coefficient, calculated with the case of 250Hz temperature can be estimated for the case of 500Hz, since the temperature coefficient is a physical property of the material.

Taking the reference T_0 in 40 °C when measured resistance (R_0) is 3.5303 Ohm, temperature can be calculated when 3.72255714 Ohms were obtained. Equations (9.3) and (9.4) show how to do it. Obtained results give an acceptable error about 1%.

$$3.72255714 = 3.53036186 * \left(1 + \alpha_{magnet} * (T - 40)\right) \tag{9.3}$$

$$T = \frac{\frac{3.72255714}{3.53036186} - 1}{\alpha_{magnet}} + 40 = 60.62°C \tag{9.4}$$

8.4.Flux weakening and flux intensifying

Last experiments done intend to give an idea about what is happening in the magnet and the magnet resistance measured when magnetic its fixed magnetic field strength is modified. Next experiment was done with three magnets, same material (neodymium) in same conditions but having different magnetic field strength, measured with a gauss-meter. One of them was heated until reach thermal demagnetization, leaving it to get ambient temperature for the experiments. And the result was that magnet resistance obtained, for the same material with different magnetization levels, changed. Resulting data for four samples taken four each magnet is show on Fig9.12

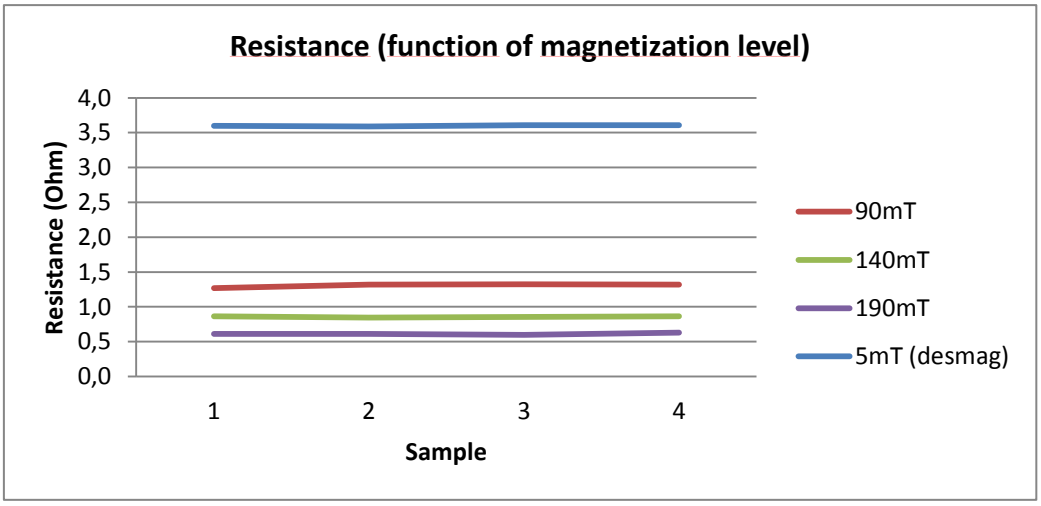

Fig9.11.Resistance obtained for same material, different magnetization level

Second experiment done for this topic intended to give results to understand how magnet resistance increase or decrease in function of the magnetic field applied. In a this system, to apply flux weakening/ intensifying to the magnet just an offset in the current is required. Positive or negative offset means weakening or intensifying, depending on the coil configuration.

Three levels of flux weakening/ intensifying were applied to the magnet. Fig9.12 shows how resistance varies for each case, and how the same values were obtained for each sample.

Last figure (Fig9.13) shows how magnet resistance varies, it can be considered linearly, for each magnetic field modification in the magnet.

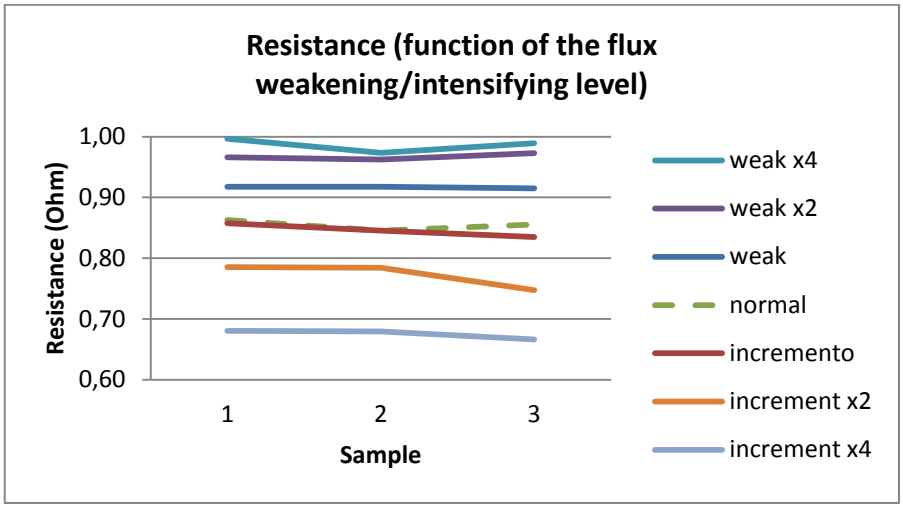

Fig9.12.Resistance obtained for same material, different magnetization level

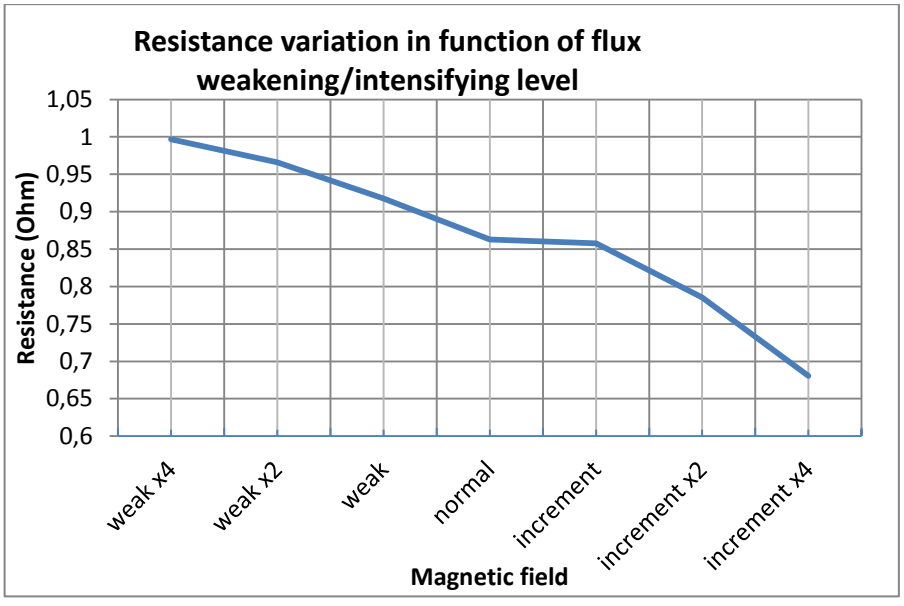

Fig9.13.Resistance obtained for same material, different magnetization level

9. Conclusions

For the measurement system, the conclusion is that taking into account some basics in electronic instrumentation, measurements can be done as precisely as wanted. Do not forget that measurement system cost increases exponentially when uncertainty gets low.

It was demonstrated that a filtering stage is needed when sensors are placed within magnetic field variations. Three kind of sensors were tested with successful an accurate results.

About the communications system, it was demonstrated that the wireless system can work close to a magnetic field variations without disturbances, both IR and Wi-Fi.

Finite element based software and practice results are not so difference when elements works under same conditions. For the case of the toroid transformer, results were more close to practice results.

E core transformer resulted useless to evaluate this method due to its vulnerability over external phenomena. With toroid Transformer, estimation temperature method can work with some constrains. Finally a dependence in the measured resistance was fond from flux modification.

With this simple topology results can be extrapolated for permanent magnet machines, to evaluate working conditions, eddy current behaviour, flux weakening or intensifying avoiding the complexity of the rotating machines.

11. Refrences

[1] H. Toda, Z. Xia, K. Atallah, and D. Howe, “Rotor eddy-current loss in permanent magnet brushless machines,” IEEE Trans. Magn., vol. 40, no. 4, pp. 2104–2106, Jul. 2004.

[2] Krishnan, R.; Vijayraghavan, P., “Fast estimation and compensation of rotor flux linkage in permanent magnet synchronous machines,” ISIE '99. Proceedings of the IEEE International Symposium on Industrial Electronics, vol.2, no., pp.661-666 vol.2, 1999.

[3] Ganchev, Martin; Umschaden, Hubert; Kappeler, Hansjoerg; , "Rotor temperature distribution measuring system," IECON 2011 - 37th Annual Conference on IEEE Industrial Electronics Society , vol., no., pp.2006-2011, 7-10 Nov. 2011.

[4] Kovačić, M.; Vražić, M.; Gašparac, I., "Bluetooth wireless communication and 1-wire digital temperature sensors in synchronous machine rotor temperature measurement," Power Electronics and Motion Control Conference (EPE/PEMC), 2010 14th International , vol., no., pp.T7-25-T7-28, 6-8 Sept. 2010.

[5] Yoshida, K.; Hita, Y.; Kesamaru, K., "Eddy-current loss analysis in PM of surface-mounted-PM SM for electric vehicles,", IEEE Transactions on Magnetics, vol.36, no.4, pp.1941-1944, Jul 2000.

[6] David Díaz Reigosa, Fernando Briz, Pablo García, Juan Manuel Guerrero, and Michael W. Degner, “Magnet Temperature Estimation in Surface PM Machines Using High-Frequency Signal Injection”, IEEE transactions on industry applications, vol. 46, no. 4, july/august 2010

[7] Fukuma, A.; Kanazawa, S.; Miyagi, D.; Takahashi, N.; , "Investigation of AC loss of permanent magnet of SPM motor considering hysteresis and eddy-current losses," IEEE Transactions on Magnetics, vol.41, no.5, pp. 1964- 1967, May 2005.

[8] F. Deng and T. W. Nehl, “Analytical modeling of eddy-current losses caused by pulse-width-modulation switching in permanent-magnet brushless direct-current motor,” IEEE Trans. Magn., vol. 34, no. 5, pp. 3728– 3736, Sep. 1998.

[10] C. Mejuto, M. Mueller, M. Shanel, A. Mebarki, M. Reekie, D.Staton, "Improved synchronous machine thermal modelling,"International Conference on Electrical Machines, ICEM 2008, pp. 1-6, Sep. 2008.

[11] Miguel A. Perez, “Instrumentación Electrónica”.

[12] “The Scientist and Engineer's Guide to Digital Signal Processing”,Second Edition, Steven W. Smith. California Technical Publishing, San Diego, California

13. INDEX OF SCHEMATICS AND PCB

DOCUMENT ONE

DOCUMENT TWO

DOCUMENT THREE

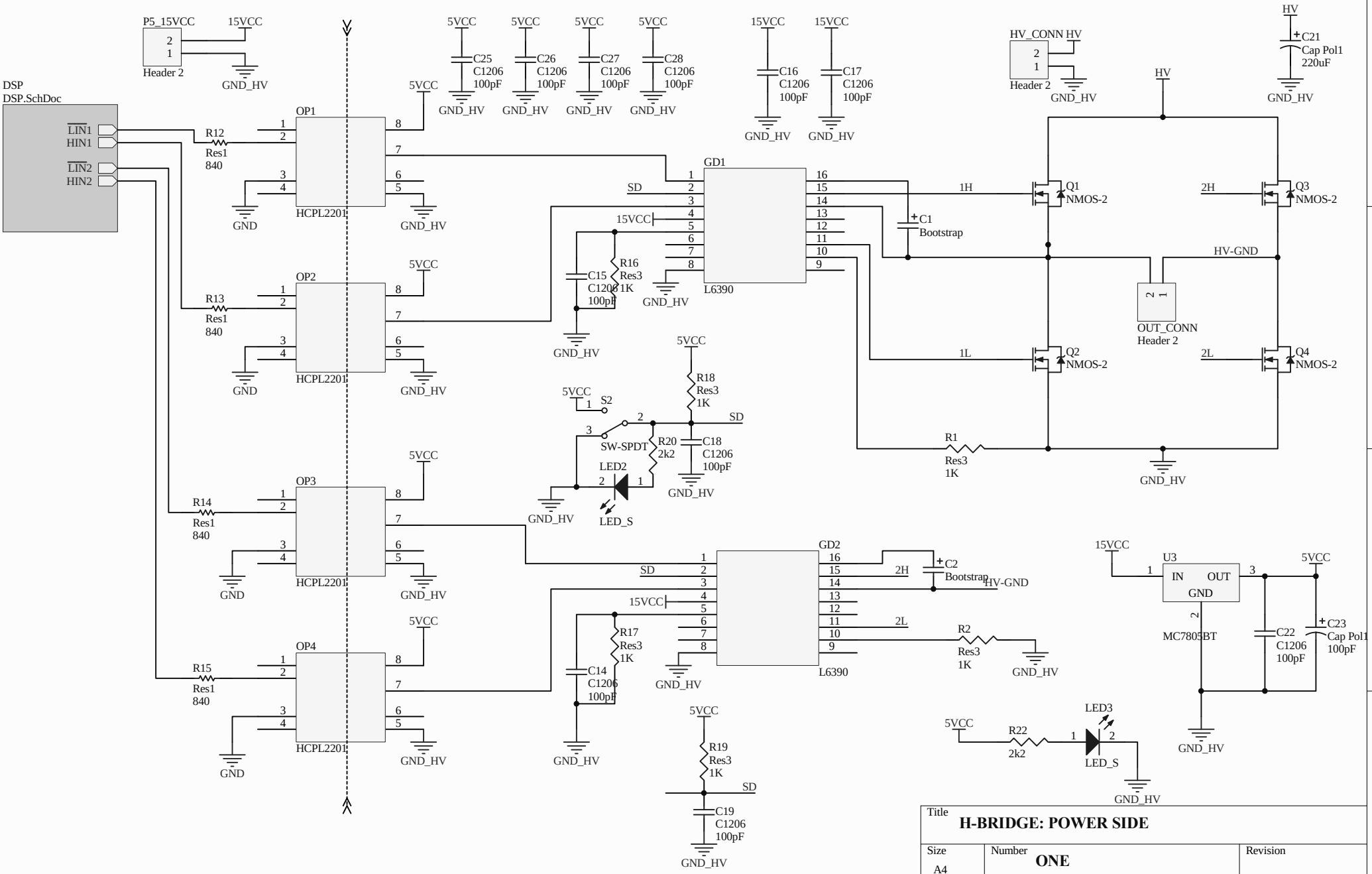
DSP
DSP.SchDoc
LIN1
HIN1
LIN2
HIN2
P5_15VCC
15VCC
Header 2
GND_HV
OP1
OP2
OP3
OP4
HCPL2201
R12
R13
R14
R15
Res1
840
GND
5VCC
C25
C26
C27
C28
C1206
100pF
C16
C17
GD1
GD2
L6390
SD
1H
2H
1L
2L
C1
C2
Bootstrap
HV-GND
HV
HV_CONN
C21
Cap Pol1
220uF
Q1
Q2
Q3
Q4
NMOS-2
OUT_CONN
R1
R2
Res3
1K
R16
R17
R18
R19
C15
C14
C19
R20
2k2
C18
S2
SW-SPDT
LED2
LED_S
LED3
R22
U3
IN
OUT
GND
MC7805BT
C22
C23
Cap Pol1
100pF
Title
H-BRIDGE: POWER SIDE
Size
A4
Number
ONE
Revision
Date:
02/07/2013
Sheet 1 of 5
File:
C:\Users\..\HBridge.SchDoc
Drawn By:
Daniel Fernández

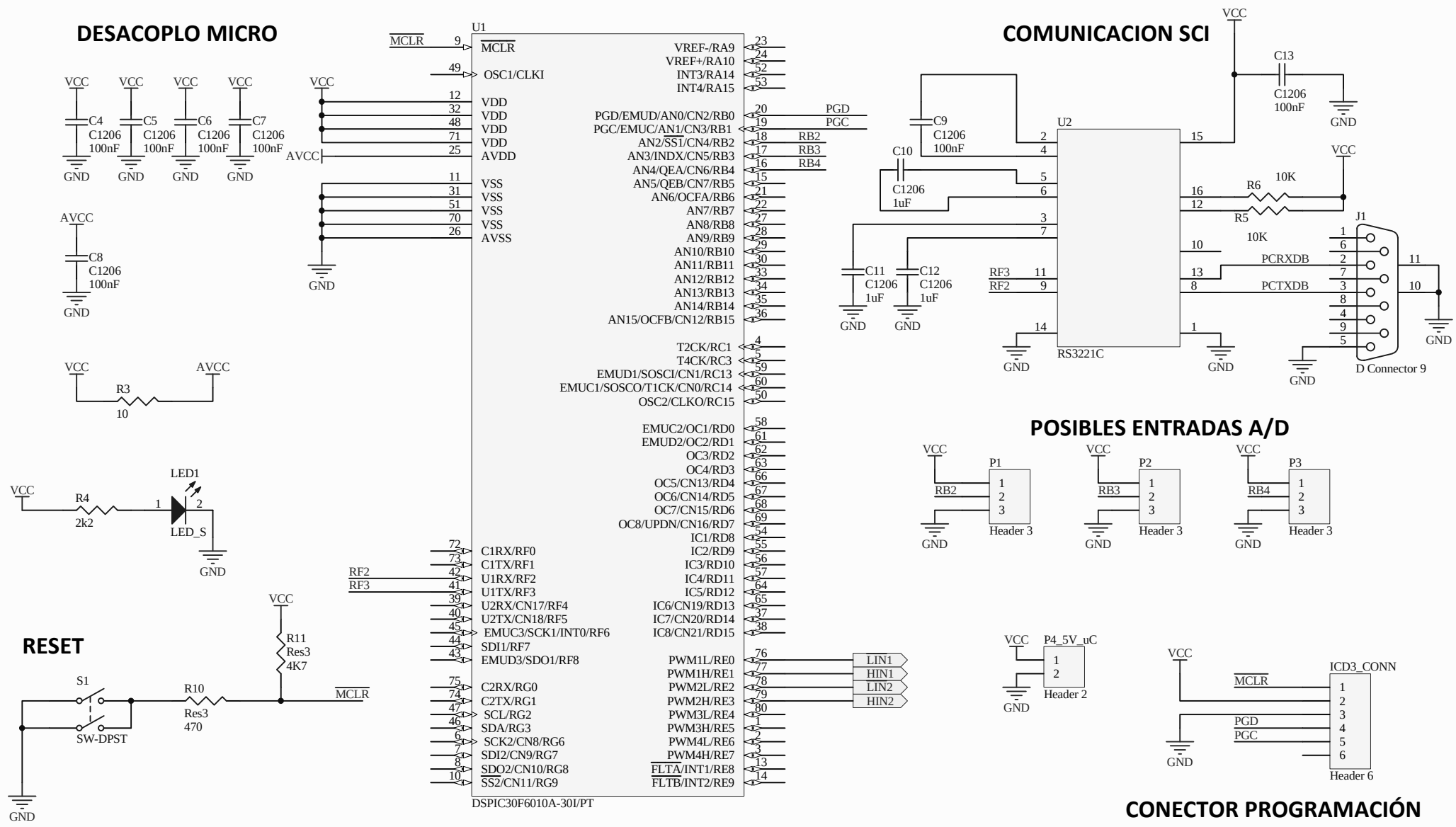

Title	**H-BRIDGE: CONTROL SIDE**
Size	A4
Number	**ONE**
Revision	
Date:	02/07/2013
Sheet **2** of **4**	
File:	C:\Users\..\DSP.SchDoc
Drawn By:	**Daniel Fernández**

control side power side

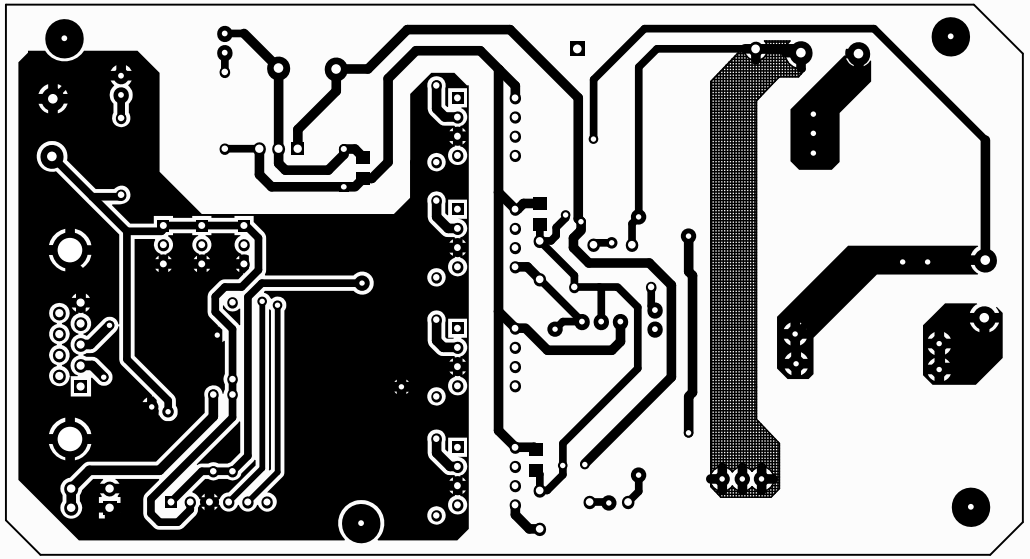

Title	**H-BRIDGE:PCB BOTTOM SIDE**		
Size A4	Number **ONE**		Revision
Date:	02/07/2013	Sheet **3** of **5**	
File:	C:\Users\..\HBridge.SchDoc	Drawn By:	**Daniel Fernández**

control side

power side

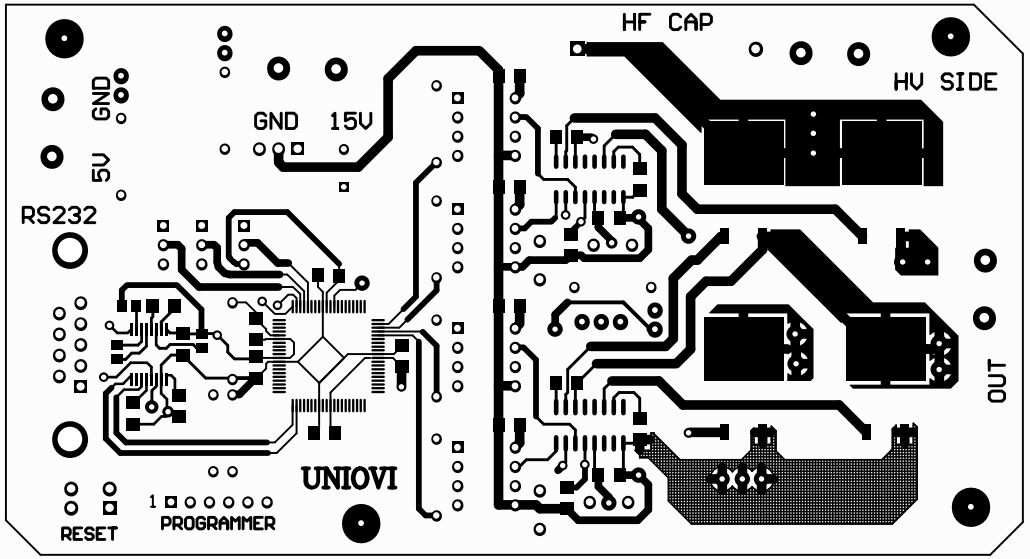

Title	**H-BRIDGE: PCB TOP SIDE**		
Size A4	Number **ONE**		Revision
Date:	02/07/2013	Sheet 4 of 5	
File:	C:\Users\..\HBridge.SchDoc	Drawn By:	**Daniel Fernández**

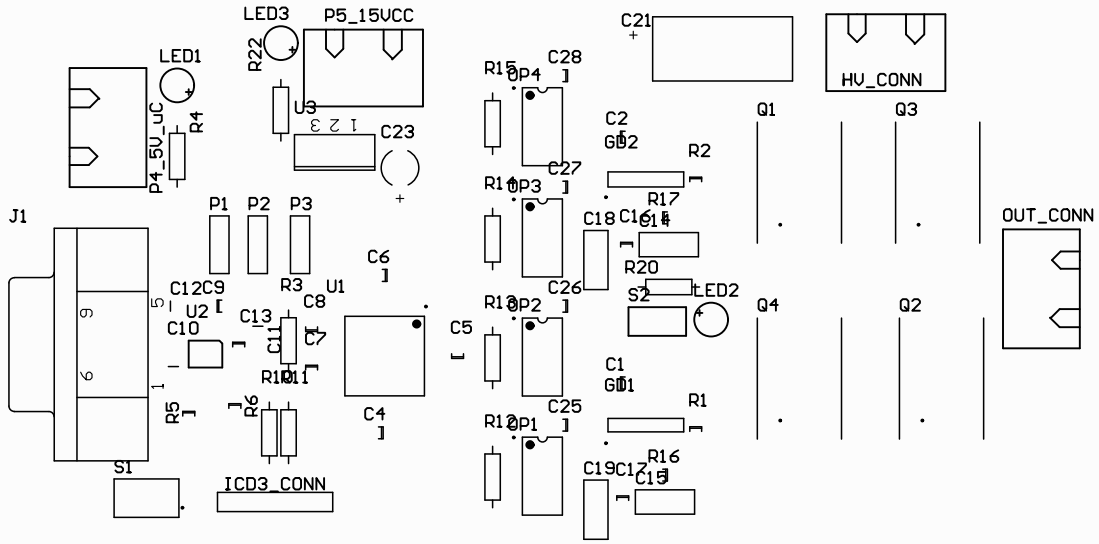

Title	**H-BRIDGE: PCB COMPONENTS**		
Size A4	Number **ONE**		Revision
Date: 02/07/2013		Sheet **5** of **5**	
File: C:\Users\..\HBridge.SchDoc		Drawn By: **Daniel Fernández**	

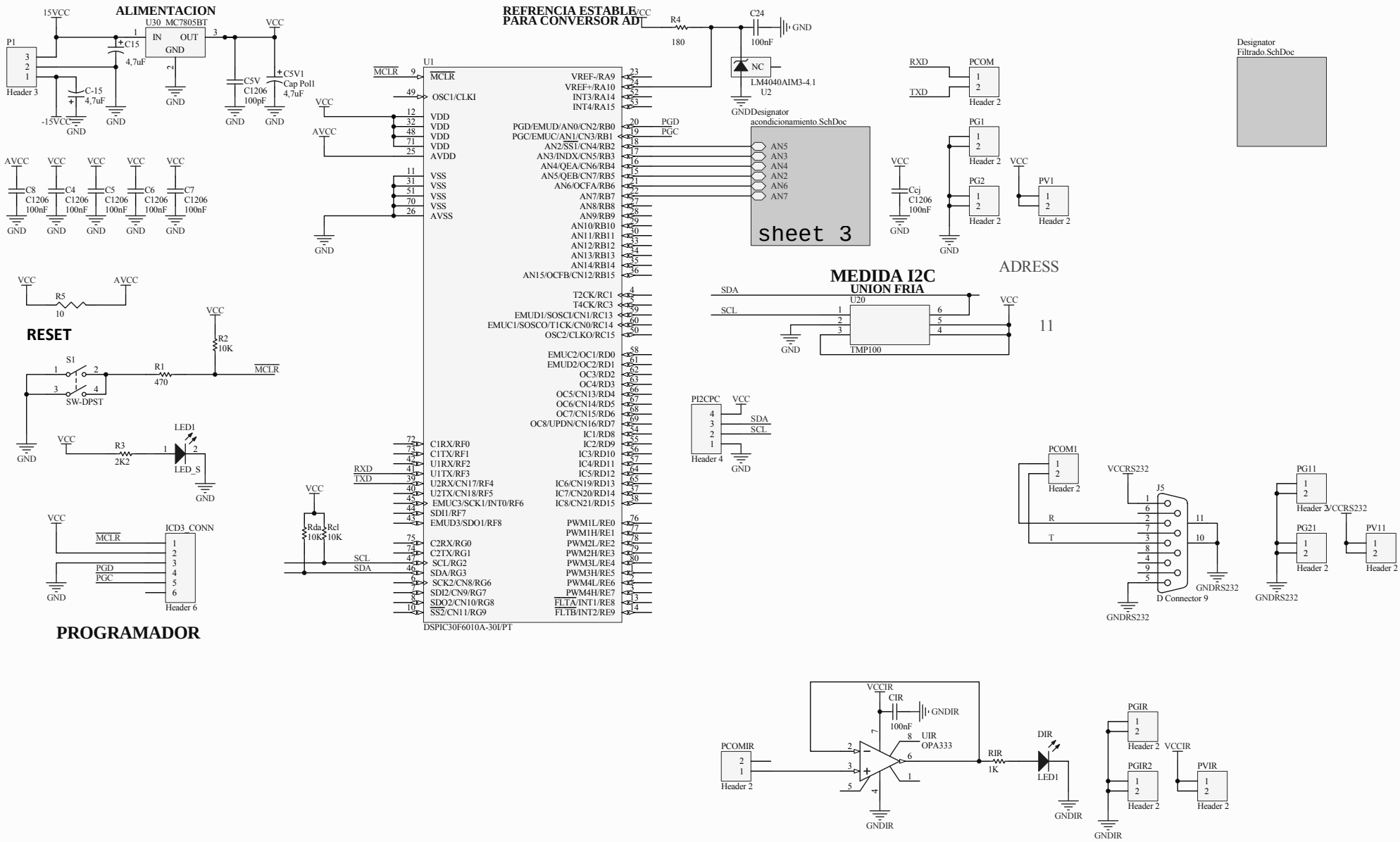

Title	TEMP MEASUREMENT: CONTROL	
Size: A3	Number: TWO	Revision:
Date: 04/07/2013		Sheet 1 of 6
File: C:\Users\..\temp.SchDoc		Drawn By: Daniel Fernández

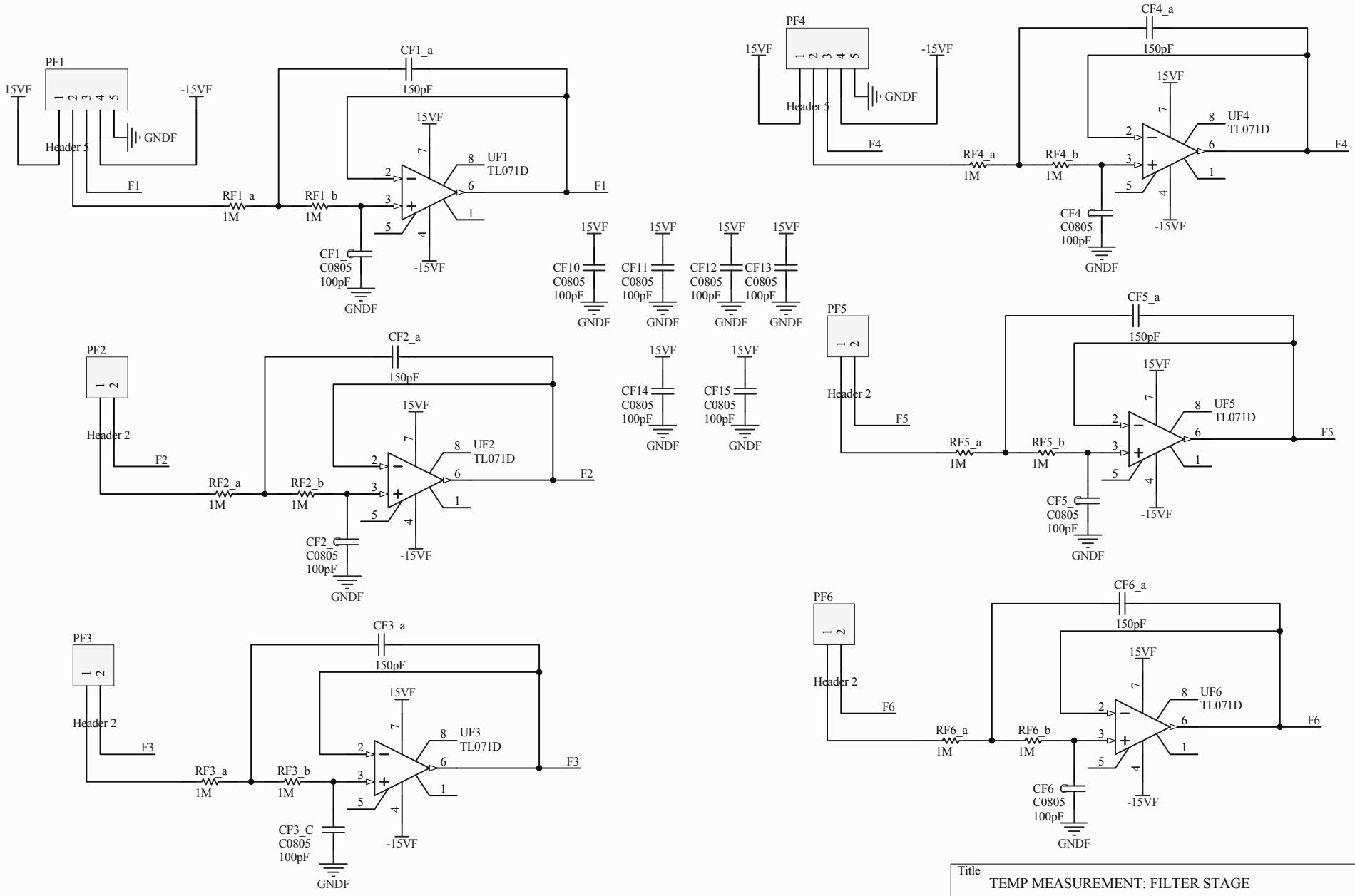

Title	TEMP MEASUREMENT: FILTER STAGE	
Size: A4	Number: TWO	Revision:
Date: 04/07/2013		Sheet2 of 6
File: C:\Users\..\Filtrado.SchDoc		Drawn By: Daniel Fernández

ALIMENTACIÓN ESTABLE PARA PUENTE WHEATSTONE

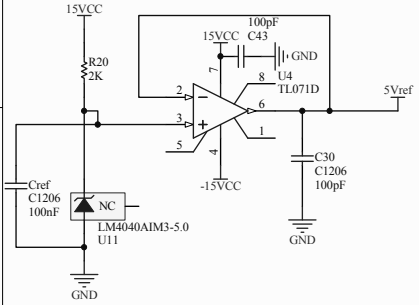

ACONDICIONAMIENTO PT100

FILTRADO pt100

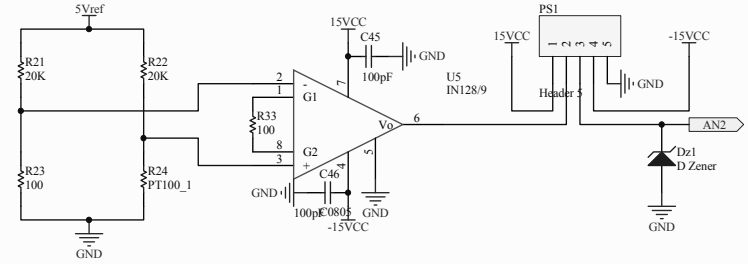

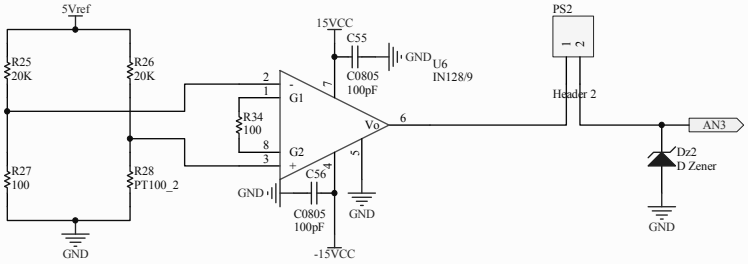

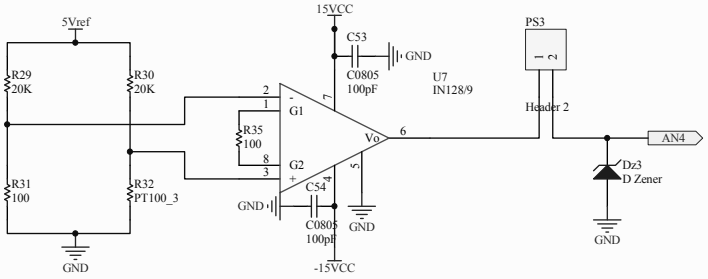

ACONDICIONAMIENTO TERMOPARES

FILTRADO TERMOPAR

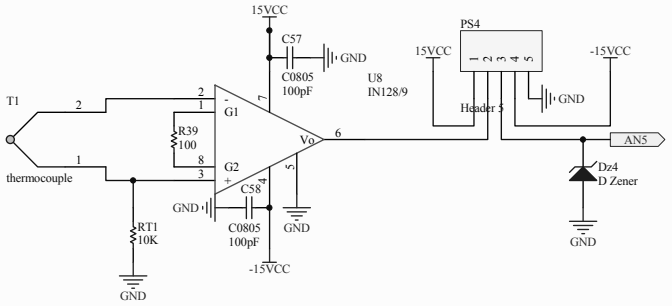

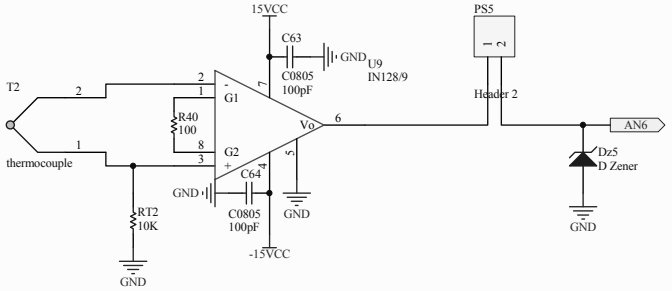

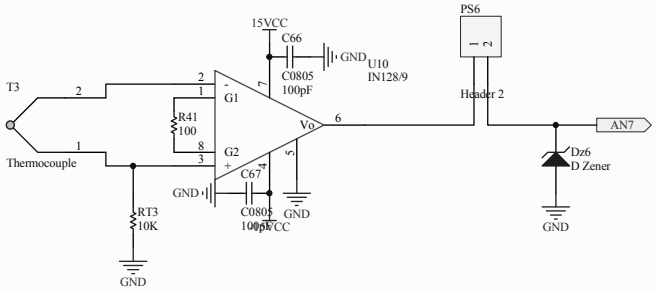

Title	TEMP. MEASUREMENT CONDITIONING STAGE	
Size A3	Number TWO	Revision
Date: 04/07/2013		Sheet 3 of 6
File: C:\Users\..\acondicionamiento.SchDoc		Drawn By:Daniel Fernández

DSC BOARD

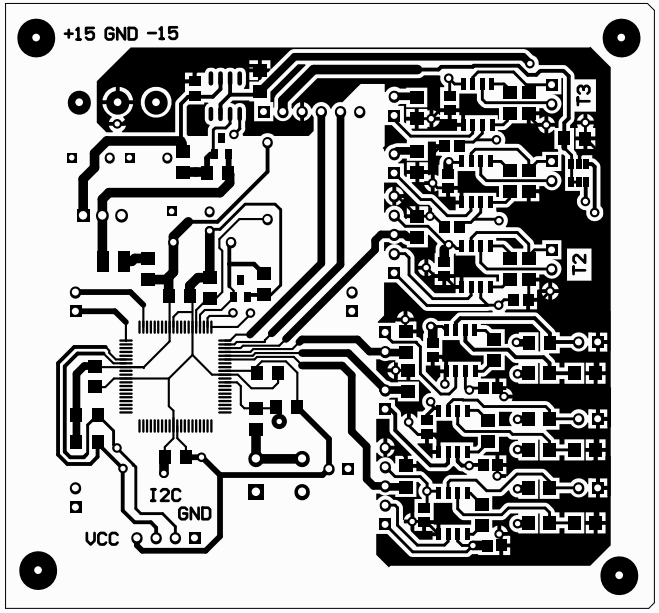

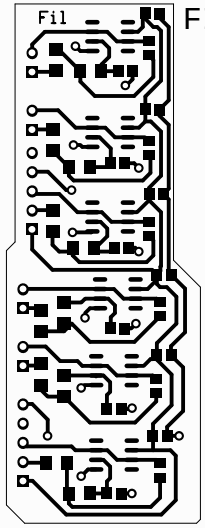

FILTER BOARD

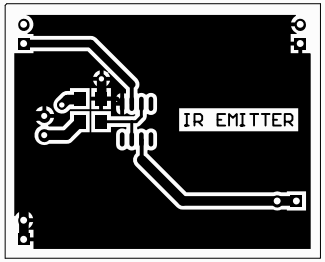

IR BASE

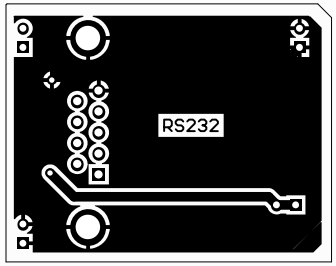

WIRE COMMUNICATION BASE

Title	**TEMP.MEASUREMENT:TOP PCB**		
Size A4	Number **TWO**		Revision
Date:	02/07/2013	Sheet **3** of **5**	
File:	C:\Users\..\HBridge.SchDoc	Drawn By:	**Daniel Fernández**

DSC BOARD

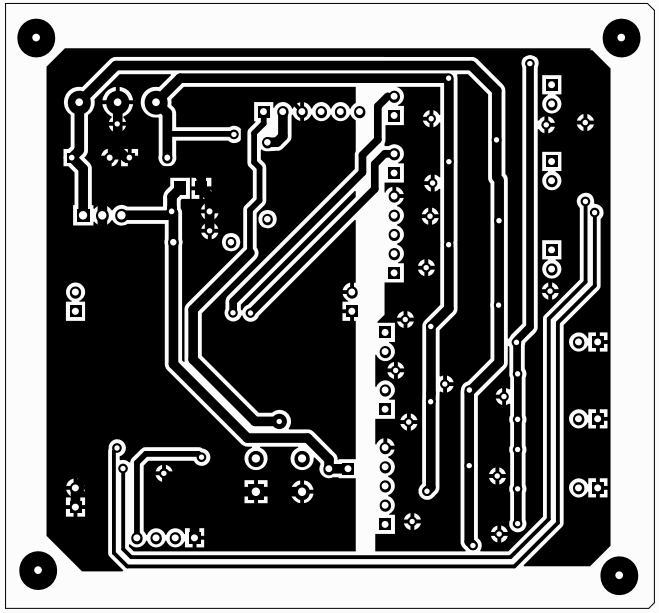

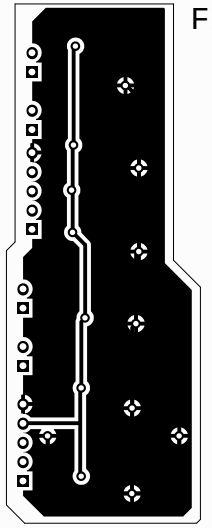

FILTER BOARD

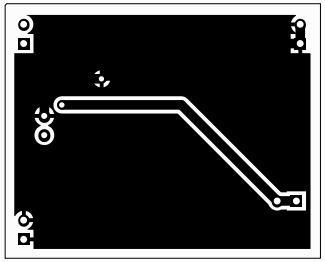

IR BASE

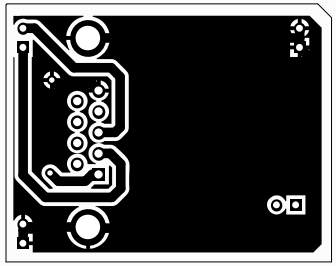

WIRE COMMUNICATIONS BASE

Title	**TEMP.MEASUREMENT: BOTTOM PCB**		
Size A4	Number **TWO**		Revision
Date:	02/07/2013	Sheet 4 of 5	
File:	C:\Users\..\HBridge.SchDoc	Drawn By:t Daniel Fernández	

DSC BOARD

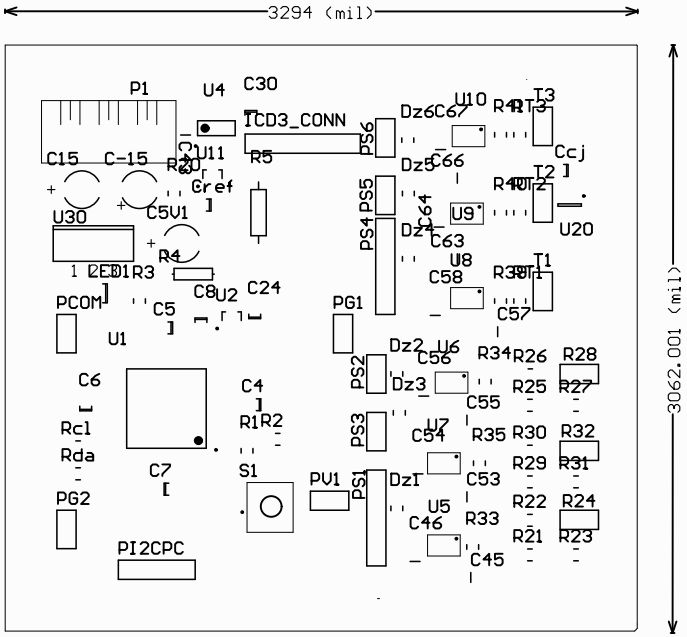

FILTER BOARD

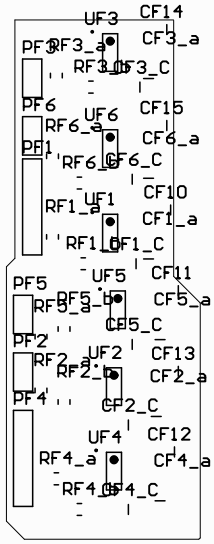

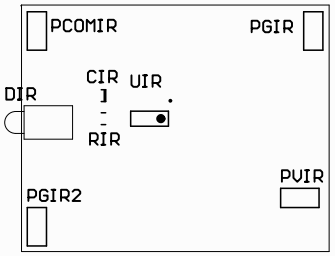

IR BASE

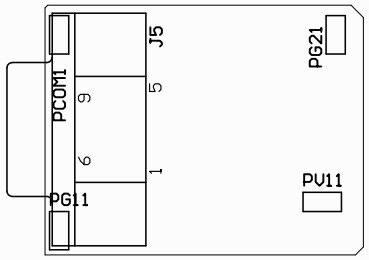

WIRE COMMUNICATION BASE

Title: **TEMP. MEASUREMENT: COMPONENTS**		
Size: A4	Number: **TWO**	Revision:
Date: 02/07/2013		Sheet **5** of **5**
File: C:\Users\..\HBridge.SchDoc		Drawn By: **Daniel Fernández**

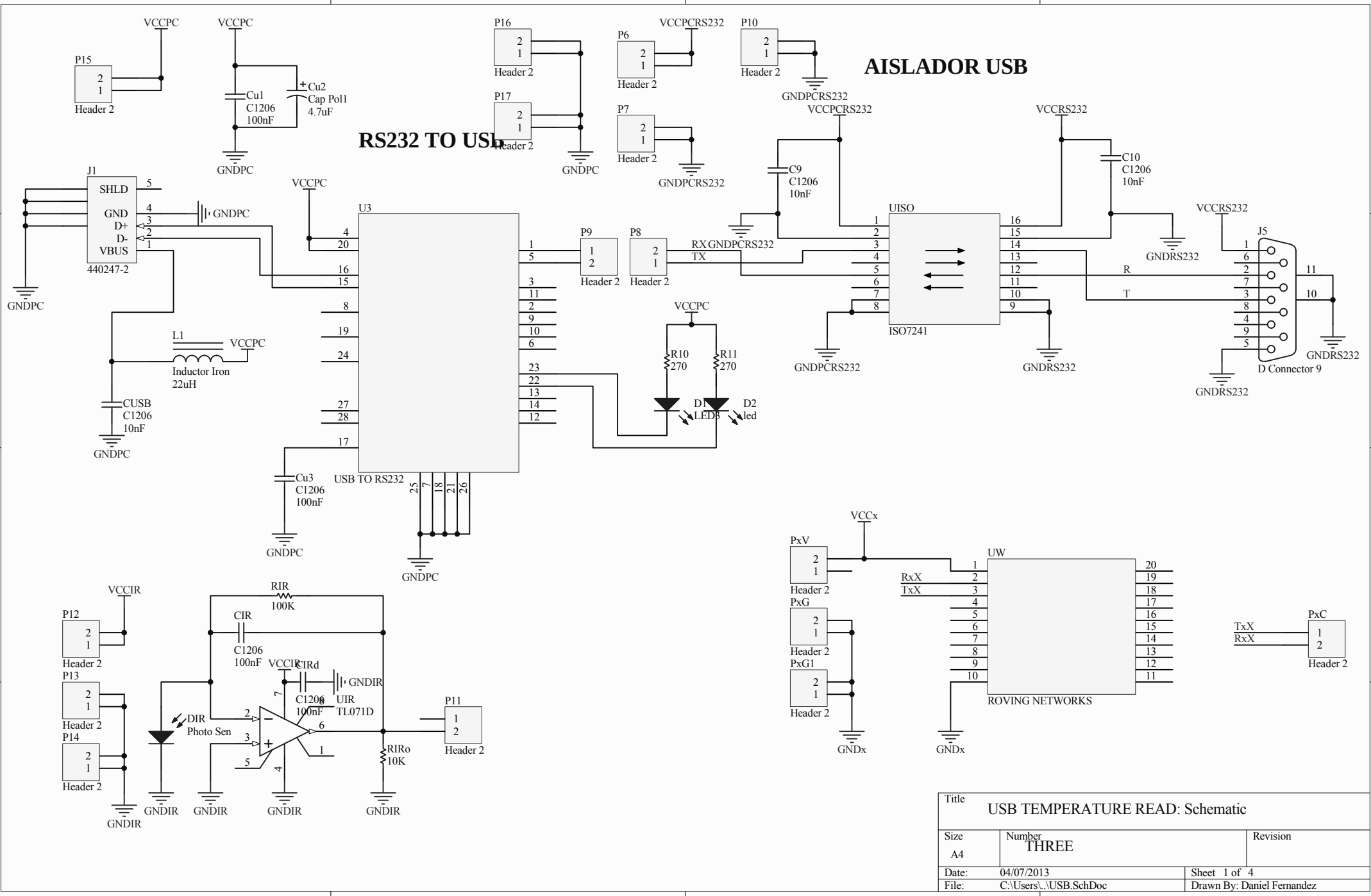
AISLADOR USB
RS232 TO USB
VCCPC
VCCPCRS232
VCCRS232
VCCIR
VCCx
GNDPC
GNDPCRS232
GNDRS232
GNDIR
GNDx
P15
Header 2
Cu1
C1206
100nF
Cu2
Cap Pol1
4.7uF
P16
P17
P6
P7
P10
J1
SHLD
GND
D+
D-
VBUS
440247-2
L1
Inductor Iron
22uH
CUSB
C1206
10nF
U3
USB TO RS232
Cu3
C1206
100nF
P9
P8
RX
TX
C9
C1206
10nF
C10
C1206
10nF
UISO
ISO7241
R10
270
R11
270
D1
LED6
D2
led
J5
D Connector 9
R
T
P12
P13
P14
RIR
100K
CIR
C1206
100nF
CIRd
C1206
100nF
UIR
TL071D
DIR
Photo Sen
RIRo
10K
P11
PxV
PxG
PxG1
UW
ROVING NETWORKS
RxX
TxX
PxC
Title
USB TEMPERATURE READ: Schematic
Size
A4
Number
THREE
Revision
Date:
04/07/2013
Sheet 1 of 4
File:
C:\Users\..\USB.SchDoc
Drawn By: Daniel Fernandez

IR BASE

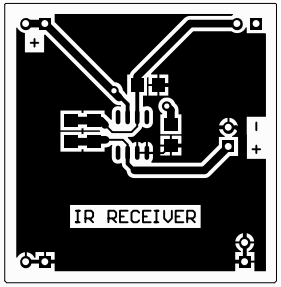

WI-FI BASE

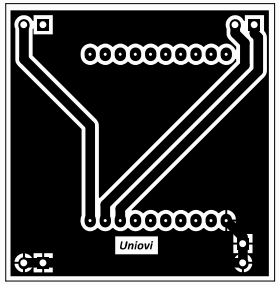

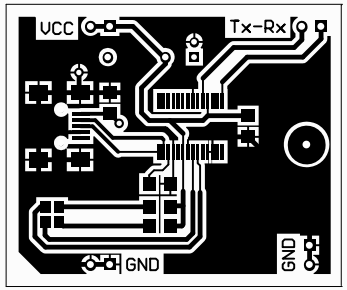

USB INTERFACE

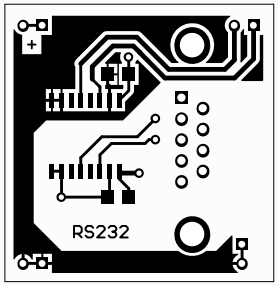

WIRE COMMUNICATION

Title: **USB TEMPERATURE READ: PCB TOP SIDE**		
Size: A4	Number: **TRHEE**	Revision:
Date: 02/07/2013		Sheet **2** of **4**
File: C:\Users\..\HBridge.SchDoc		Drawn By: **Daniel Fernández**

IR BASE

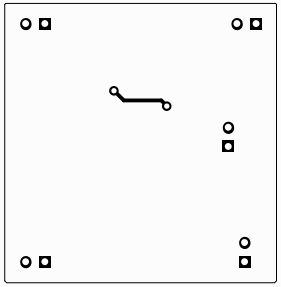

WI-FI BASE

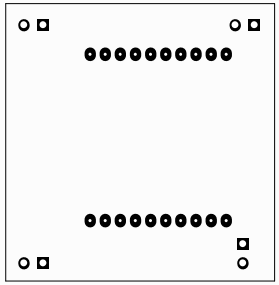

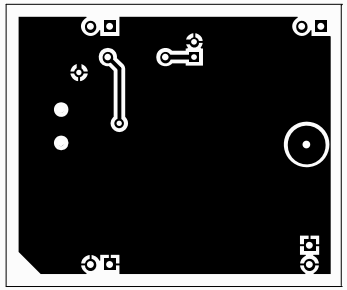

USB INTERFACE

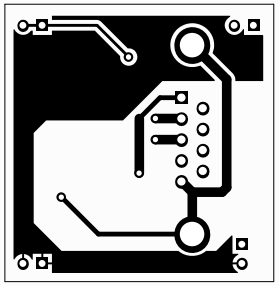

WIRE COMMUNICATION

Title	**USB TEMPERATURE READ: PCB BOTTOM**		
Size: A4	Number: **TRHEE**		Revision:
Date: 02/07/2013		Sheet **3** of **4**	
File: C:\Users\..\HBridge.SchDoc		Drawn By: **Daniel Fernández**	

IR BASE

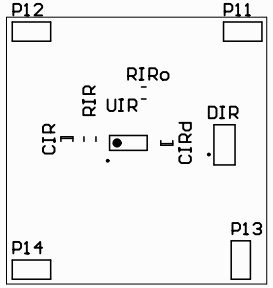

WI-FI BASE

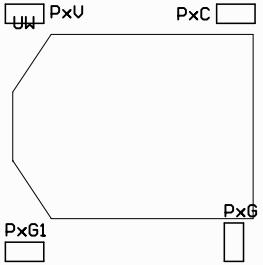

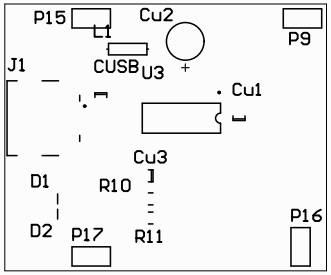

USB INTERFACE

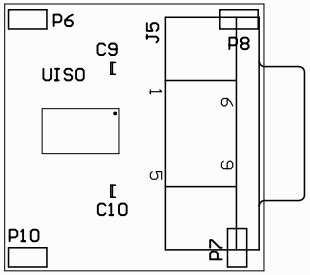

WIRE COMMUNICATION

Title	**USB TEMPERATURE READ: COMPONENTS**		
Size A4	Number **TRHEE**		Revision
Date:	02/07/2013	Sheet 4 of 4	
File:	C:\Users\..\HBridge.SchDoc	Drawn By:	**Daniel Fernández**

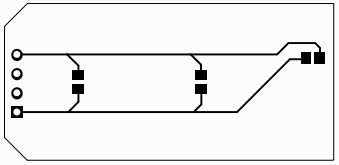

Title	**SENSOR PCB: I2C**		
Size: A4	Number: **FOUR**		Revision:
Date:	02/07/2013	Sheet **1** of **4**	
File:	C:\Users\..\HBridge.SchDoc	Drawn By:	**Daniel Fernández**

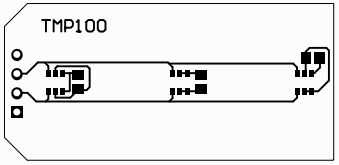

Title	**SENSOR PCB: I2C**	
Size: A4	Number: **FOUR**	Revision:
Date: 02/07/2013		Sheet **2** of **4**
File: C:\Users\..\HBridge.SchDoc		Drawn By: **Daniel Fernández**

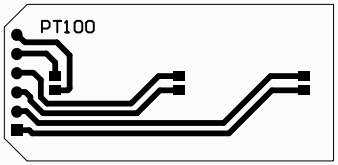

Title	**SENSOR PCB: PT100**	
Size: A4	Number: **FOUR**	Revision:
Date: 02/07/2013		Sheet **3** of **4**
File: C:\Users\..\HBridge.SchDoc		Drawn By: **Daniel Fernández**